The Spectral Characteristics of Lunar Agglutinates: Visible–Near-Infrared Spectroscopy of Apollo Soil Separates

Chanud N. Yasanayake[1,2], Brett W. Denevi[1], Takahiro Hiroi[3], Brad. L. Jolliff[4], Anna C. Martin[1], Annabelle L. Gao[3,5], Margaret L. Zhang[6,7], Lucas M. Bloom[8,9], and Samuel J. Lawrence[10]

[1]Johns Hopkins University Applied Physics Laboratory. [2]Johns Hopkins University. [3]Brown University. [4]Washington University in St. Louis. [5]Marriotts Ridge High School. [6]University of North Carolina at Chapel Hill. [7]Mount Hebron High School. [8]University of Alabama. [9]Severna Park High School. [10]NASA Johnson Space Center.

Corresponding authors: Chanud N. Yasanayake (chanud@jhu.edu), Brett W. Denevi (brett.denevi@jhuapl.edu)

Key Points:

- We measured reflectance spectra of agglutinates and non-agglutinates separated from six lunar soils of varying composition and maturity.
- Spectral comparisons suggest that spectral reddening of mature soils is expressed mainly via agglutinates (for the size fractions measured).
- These findings reframe our understanding of the relative spectral roles of agglutinates and soil grain rims in weathered lunar soils.

Abstract

The lunar surface evolves over time due to space weathering, and the visible–near-infrared spectra of more mature (i.e., heavily weathered) soils are lower in reflectance and steeper in spectral slope (i.e., darker and redder) than their immature counterparts. These spectral changes have traditionally been attributed to the space-weathered rims of soil grains (and particularly nanophase iron therein). However, understudied thus far is the spectral role of agglutinates—the agglomerates of mineral and lithic fragments, nanophase iron, and glass that are formed by micrometeoroid impacts and are ubiquitous in mature lunar soils. We separated agglutinates and non-agglutinates from six lunar soils of varying maturity and composition, primarily from the 125–250 μm size fraction, and measured their visible–near-infrared reflectance spectra. For each soil, agglutinate spectra are darker, are redder, and have weaker absorption bands than the corresponding non-agglutinate and unsorted soil spectra. Moreover, greater soil maturity corresponds to darker agglutinate spectra with weaker absorption bands. These findings suggest that agglutinates (rather than solely the space-weathered rims) play an important role in both the darkening and reddening of mature soils—at least for the size fractions examined here. Comparisons with analog soils suggest that high nanophase iron abundance in agglutinates is likely responsible for their low reflectance and spectrally red slope. Additional studies of agglutinates are needed, both to more comprehensively characterize their spectral properties (across size fractions and in mixing with non-agglutinates) and to assess the relative roles of agglutinates and rims in weathering-associated spectral changes.

Plain Language Summary

In scientific study of the Moon, one key focus is surface processes: how do physical and chemical properties of the Moon's surface change over time due to weathering (e.g., bombardment by micrometeoroids and by particles from the Sun)? Such investigations provide valuable insights into the Moon's history (such as the ages of impact craters) that are often deduced from measurements of reflected light; as a soil is weathered it reflects light differently, which manifests visually as a progressive darkening of the soil. This phenomenon had primarily been attributed to weathering-associated development of rims on individual soil grains, but in this work we explored an alternative cause: soil particles known as agglutinates (misshapen, vesicular agglomerates of mineral fragments, iron, and glass that form due to weathering processes). We isolated agglutinates of six soil samples from the Moon and measured how they reflect light. We find that they reflect light in patterns reminiscent of how the Moon's surface does when weathered. These findings suggest that agglutinates play a more important role than previously thought in determining the light-reflecting properties of the Moon's surface, thus warranting greater and more nuanced consideration in future studies of how the Moon's surface changes over time.

1 Introduction

The lunar surface evolves over time, gradually changing as it endures a continual bombardment by micrometeoroids and the solar wind—chief among processes that are collectively known as space weathering. These weathering processes impart observable changes onto lunar soil that alter how it reflects light. At visible–near-infrared (Vis–NIR) wavelengths, mature (i.e., heavily weathered) lunar soils are lower in reflectance, have a steeper (redder) spectral slope, and have weaker crystal field absorption bands than their less-weathered counterparts (e.g., Adams & McCord, 1970, 1971a, 1971b, 1973; Pieters et al., 1993; Taylor et al., 2001a, 2001b). It is an ongoing effort dating back many decades to link these spectral changes to physical and chemical changes in the lunar soil and, in turn, link the physical and chemical changes to specific causative processes.

The physical and chemical changes that have the largest spectral effects include the comminution of rocks into a fine particulate, the conversion of crystalline minerals into less ordered and glassy materials, and changes in the oxidation state of iron (e.g., the reduction of ferrous iron (FeO) to metallic iron (Fe^0)) (e.g., Hapke, 2001; Lucey et al., 2006; Pieters & Noble, 2016). All three of these processes are observed at the individual lunar soil (regolith) particle level. A single regolith particle is on average ~70 μm in size (Carrier, 2003) for mature soils, the result of long-term impact bombardment and regolith gardening. Each particle in a mature soil typically has an amorphous rim or surficial coating up to ~200 nm thick (Keller et al., 2021). This rim can either be due to damage to the crystal structure caused by energetic charged-particle radiation (largely sourced from the Sun, i.e., the solar wind), or can be depositional, from condensation of impact-generated vapor or solar-wind ion sputtering (see overview in Denevi et al., 2023). While differences in grain size and crystallinity have modest effects on spectral reflectance, the depositional rims have been the focus of many studies because they contain small (<10 nm) spherules of iron (Keller & McKay, 1993, 1997) that increase in abundance with maturity and cause substantial changes in reflectance (e.g., Hapke, 1973; Hapke et al., 1975; Cassidy & Hapke, 1975; Hapke, 2001; Pieters et al., 1993). This population of small iron grains is often called nanophase iron (npFe or $npFe^0$) or submicroscopic iron (SMFe). While this iron is typically reduced, metallic iron (Fe^0), it can be found in a range of oxidation states (Fe^0, Fe^{2+}, or Fe^{3+}) (Keller and Clemett 2001; Thompson et al., 2016; Burgess and Stroud, 2017; Burgess and Stroud, 2018), so in this work we use the terms nanophase iron or npFe (rather than $npFe^0$).

While the depositional rims containing npFe have been the most recent focus of attention in terms of causing spectral changes (e.g., Pieters et al., 1993; Christoffersen et al., 1996; Keller et al., 2021), another soil particle plays an important role: agglutinates. Agglutinates are misshapen, vesicular agglomerates of mineral and lithic fragments, bound together by glass (Figure 1). They form when an impact event melts regolith, which incorporates clasts of other regolith grains and releases trapped solar wind volatiles to create vesicles (Basu et al., 2002 and references therein). Agglutinates range in size from ~tens of microns to mm-scale, and in mature soils they can comprise up to 60% of the soil volume (McKay et al., 1991). Their abundance and the fact that they are so visually dark suggests that agglutinates have a substantial influence on spectral reflectance. Initially their dark brown appearance was attributed to the glass itself (e.g., Conel & Nash, 1970; Nash & Conel, 1973; Adams & McCord, 1971a), but subsequent work showed that glass melted in a vacuum is not inherently low in reflectance (Wells & Hapke, 1977). Instead, the spectral properties of agglutinates are strongly affected by their substantial

population of npFe. This iron is found within the flash-melted glass (Figure 1). Some of the npFe may be from the npFe-rich rims on soil grains that have been incorporated into the melt. It is not known whether melting/vaporization alone results in the creation of additional npFe via the reduction of FeO to Fe (with O lost as a volatile species; e.g., Hapke, 1975, 2001; Keller & McKay, 1993, 1997) or whether implanted solar wind H^+ aids in the reduction process (forming OH^- or H_2O; Housley et al., 1972, 1974; Morris, 1977, 1980; Taylor & Cirlin, 1985; Denevi et al., 2023).

However it is formed, the abundance of npFe in agglutinates is so high that agglutinates can be separated magnetically from most other soil components (e.g., Adams & McCord, 1973; Via & Taylor 1976a, 1976b), and the npFe spans a much larger range of sizes than in depositional rims (mean size 120 nm vs. 3 nm; James et al., 2002, Keller & Clemett, 2001), possibly because npFe grains grow with repeated thermal shocking (Thompson et al., 2017). The spectral effects of npFe are now known to vary with abundance and size (Noble et al., 2007); greater abundance and larger size can both lead to lower reflectance and a shallower spectral slope. Large grains (greater than ~40 nm; sometimes referred to as microphase Fe) are thought to "darken without reddening" and agglutinates have often been described as only lowering the overall reflectance of a soil, without changing its spectral slope due to their large average npFe grain size (e.g., Britt & Pieters, 1994; Keller et al., 1998; Noble et al., 2007; Pieters & Noble, 2016).

Although agglutinates are a major component of mature soils, their spectra have not been extensively studied. In fact, agglutinate reflectance spectra have only been published for a single lunar soil, the high-titanium Apollo 11 sample 10084 (Pieters et al., 1993; Keller et al., 1998). The lack of in-depth spectral studies of agglutinates is somewhat surprising, until one learns just how tedious it is to separate agglutinates from lunar soil (see Section 2.2). Still, given the dearth of comprehensive studies of agglutinate spectral properties thus far, there remain many open questions regarding the basic nature of these particles. For example, do all lunar agglutinates have comparable spectra, or do they differ significantly based on the composition of the regolith from which they were produced? And, while it is well-documented that agglutinates increase in abundance as soils are progressively weathered (e.g., Taylor et al., 2001a, 2001b, 2010), do the agglutinate particles themselves evolve with increasing maturity? What is the overall spectral contribution of agglutinates vs. depositional rims to lunar spectra?

Here we have extended the existing characterization of agglutinates and contributed to answering these questions by measuring the spectral properties of (primarily 125–250 μm) agglutinate and non-agglutinate particles isolated from six different Apollo lunar soil samples: 14259, 15041, 61141, 62231, 67461, 79221. We have similarly measured each soil after sieving (e.g., to 125–250 μm) but prior to sorting into agglutinate and non-agglutinate separates, and we henceforth refer to this soil as the unsorted soil. By comparing the reflectance spectra of agglutinates, non-agglutinates, and unsorted soils of varying composition and maturity, we seek to contribute to the effort to understand how space weathering proceeds on the Moon and how to interpret spectral changes related to maturity.

2 Methods

2.1 Lunar soil selection

In order to characterize agglutinates, we selected six lunar regolith samples (<1 mm fines) for this study: 14259, 15041, 61141, 62231, 67461, and 79221 (Table 1). These samples were chosen for their wide range in soil composition and maturity, and because they have been extensively characterized by previous studies in terms of mineralogy, chemistry, maturity, and spectral properties (Taylor et al., 2001a, 2001b, 2010; Morris, 1978; Pieters et al., 2002).

Soil	Soil type	Provenance[a]	FeO (wt%)[b]	TiO_2 (wt%)[b]	I_S/FeO[c]	Maturity	Agglutinate abundance (%)[d]
67461	Low-Fe highlands	Fillet of boulder, rim of North Ray Crater	4.2	0.4	25	Immature	25
61141	Low-Fe highlands	30m from rim of Plum Crater	4.8	0.6	56	Submature	50
62231	Low-Fe highlands	Rim of Buster Crater	4.9	0.6	91	Mature	50
14259	Moderate-Fe nonmare	Top 1cm of soil, 100m west of lunar module	9.5	1.8	85	Mature	61
15041	Low-Ti mare	Top of trench dug near Station 8	14.2	1.8	94	Mature	51
79221	High-Ti mare	Top 2cm of trench dug near Van Serg Crater	14.0	6.4	81	Mature	47

Table 1. Lunar regolith samples examined in this study.
[a] Meyer (2005); reports for soils 67461, 61181, 62231, 14259, 15030, 79221. [b] Taylor et al. (2001a, 2001b, 2010); weight percent in <45 μm size fraction. [c] Morris (1978); I_S/FeO for <250 μm size fraction. [d] Taylor et al. (2001a, 2001b, 2010); modal (volume) abundance of agglutinitic glass in the 20–45 μm size fraction.

The range in lunar soil composition is represented by samples that are of comparable maturity, but that originate from low- and high-titanium mare (15041 and 79221, respectively), nonmare (14259), and highlands (62231) regions. This range of compositions expands beyond previous published work, which focused only on agglutinates from a high-titanium mare region (sample 10084, in Pieters et al., 1993).

The suite of Apollo 16 soils (67461, 61141, and 62231) represent the range of soil maturity found on the Moon. The maturity of lunar samples is commonly quantified as I_S/FeO: the ferromagnetic resonance intensity (I_S) of the soil's <250 μm size fraction normalized to its FeO concentration (Housley et al., 1973, 1974, 1975; Morris, 1976, 1978). The normalization of

I_S to FeO is necessary because the I_S signal is produced by nanophase iron (npFe) particles in the diameter range of 4–33 nm (Housley et al., 1976, Morris, 1980), and the concentration of npFe in the soil depends both on the degree of surface exposure (which reduces Fe^{2+} in the soil to Fe^0) as well as on the concentration of FeO in the soil (which is the source of the Fe^{2+}). By normalizing I_S to the FeO concentration in the soil, the maturity of soils of differing composition can be compared (Housley et al., 1973, 1974, 1975).

Lunar soils are categorized based on I_S/FeO value as immature (I_S/FeO < 30), submature (30 < I_S/FeO < 60), or mature (I_S/FeO > 60). Sample 62231, like the samples used here from Apollo 14, 15, and 17, is mature (Table 1). Sample 61141 is submature and 67461 is immature. All three samples are from the highlands, although each is from the rim of a different crater at the Apollo 16 landing site, allowing for an assessment of if/how agglutinate spectral properties vary with maturity.

Note that the I_S/FeO values cited in Table 1, from Morris (1978), are based on measurements of a broader size fraction (<250 μm) than the size fraction of the separated agglutinates (125–250 μm). This means that the I_S/FeO values may not *directly* correspond to the physical properties of the soils in our study, but they are still a valid tool for comparing soils to one another and considering *relative* differences in maturity, under the assumption that, for any two soils, a soil with greater I_S/FeO value for the <250 μm size fraction also has greater I_S/FeO value for any other size fraction.

2.2 Separating agglutinates

In past work, a variety of methods have been used to isolate agglutinates from regolith samples. Separation of particles based on magnetic susceptibility is effective to some degree, as demonstrated by Adams and McCord (1973), since the iron-metal-rich agglutinates tend to be the most magnetic particles in the soil. However while magnetic separation can yield an agglutinate-rich separate, it may contain 10–20% non-agglutinates that are highly magnetic while excluding agglutinates that are less magnetic (ranging from <5% to >20% of the remnant soil) (Via & Taylor, 1976a). Pieters et al. (1993) bypassed this issue in their study of sample 10084 by hand picking individual agglutinates, which, while time-intensive, presumably produced a purer agglutinate separate.

In this work, we used two different methods of separating agglutinates and compared their effectiveness. In both cases we first isolated the 125–250 μm size fraction of each regolith sample by sieving and then rinsing with ethanol to remove any clinging fines. This size fraction was the smallest we found to be practicable to manipulate with tweezers (as static causes smaller particles to jump and stick to tools). For each sample we started with an initial mass of 2 g, with the 125–250 μm size fraction constituting ~15% of the total sample mass. We obtained two 2-g splits of sample 62231, in order to test both agglutinate separation methods on the same material (see below). We also requested a second 2-g split of sample 67461 because the agglutinates make up a smaller fraction of this immature sample, and the mass of agglutinates separated from the initial split was too small for the acquisition of reflectance spectra with the setup used.

The first agglutinate separation method was manual, similar to the method of Pieters et al. (1993), wherein we selected individual agglutinate particles from the sample using tweezers. To do so, we poured a small portion of the sieved regolith sample into a dish. We then observed the sample under a binocular microscope and identified agglutinates based on their appearance: irregular shape, vesicular, typically brown in color, and a surface texture that varies from rough to glassy, interspersed with mineral fragments (Figure 2). All other particles were deemed "non-agglutinates". We took care to gently grip the agglutinates with the tweezers, as the friable particles were liable to break apart if gripped too strongly, and moved them to a separate container. These particles constituted the manually separated agglutinates, and we sorted through the remainder of the soil until the point of diminishing returns (i.e., continued searching revealed few additional agglutinates). This remainder of the soil was the non-agglutinates. We refer to this first separation method as the manual method.

We note that there is some ambiguity in whether a given particle is an agglutinate or not. Because agglutinates include mineral and lithic fragments bound by impact melt glass, there are some regolith particles that appear to be, e.g., largely a mineral fragment with only a small portion of the particle having the characteristic shiny surface and irregular shape that results from impact melt glass. There are also a number of particles that may best be described as dark, glassy melt breccias, and that appear to contain a smaller portion of glass and have angular shapes. These particles have sometimes been referred to as "dark matrix breccias" or lumped together with agglutinates as "fused soil components" (e.g., Adams & Charette, 1975; Vaniman & Papike, 1977). Thus, when performing the manual separation, we took pains to be consistent in what was included as an agglutinate and what was excluded as a non-agglutinate (Figure 2).

The second separation method began with magnetic separation. We poured the sieved regolith sample into a Frantz magnetic separator where the particles flowed down a chute (25° forward angle, 15° side angle) past a magnet. The magnet current was held at 0.5 A for all samples except the immature sample 67461, which required a stronger current of 1.0 A to effectively separate agglutinates. We used vibration pulses of the feed and chute to ensure that most particles fell into the two bins at the end of the chute, and we considered everything that went down the chute to be the low-agglutinate remnant (i.e., Figures 3A, 3D combined with Figures 3B, 3E). The most magnetic particles were held suspended in the chute by the magnet; after setting aside the low-agglutinate remnant we gathered the magnetically suspended particles after slowly reducing the current to zero. These particles constituted our agglutinate-rich separate (Figures 3C, 3F). We found that this agglutinate-rich separate contained ~15–45% agglutinates (poorer than the 80–90% purity obtained by Via and Taylor (1976b) using a hand magnet) while the low-agglutinate remnant contained >90% non-agglutinates (comparable to the 80–95% purity of Via and Taylor (1976b)). We then employed the manual separation method to improve the purity of the agglutinate-rich separate, both removing any non-agglutinates from the separate and also recovering agglutinates from the low-agglutinate remnant to leave just non-agglutinates (Tables S1, S2). We refer to this second separation method as the magnetic–manual method.

Note that the magnetic separation step in our magnetic–manual method differs from that used by Adams and McCord (1973). While we poured our regolith samples down the chute of the magnetic separator, they poured their samples down an ethanol-filled pipette attached to their magnetic separator. We initially tried their method, but had difficulty achieving successful separation; the process was time-intensive, the soil particles tended to get stuck on the pipette

valve, and the agglutinate-rich separate yielded by this method still included a substantial number of non-agglutinates (particularly, dark, glassy melt breccia particles). Given these difficulties of using the pipette, we opted for a simpler magnetic separation step using the magnetic separator chute instead of a pipette, as already described.

The magnetic–manual method does not resolve all ambiguity in determining what is an agglutinate or not. The current selected for the magnet affects which regolith particles end up on either side of the dividing line, and the existence of the intermediate population of regolith particles (Figures 3B, 3E) suggests again there is not a clear cut-off. Further, because the magnetic separation is imperfect, one must still manually inspect and decide on whether or not each particle is an agglutinate. This is unfortunate as it is this manual separation step that makes both methods time-intensive (taking tens of hours to separate out ~50 mg of agglutinate particles). However the magnetic–manual method was still noticeably faster than the manual method; by initially concentrating agglutinates via the magnetic separation step, far fewer particles needed to be separated during the manual separation step.

The two separation methods were independently applied to soil 62231. This yielded two agglutinate separates: one separated using the manual method and one using the magnetic–manual method. Measurements of these two 62231 agglutinate separates, identical except for sorting method, allow us to compare the effectiveness of the two separation methods.

2.3 Collecting reflectance spectra

We collected reflectance spectra of the samples at the Reflectance Experiment Laboratory (RELAB) at Brown University (Milliken et al., 2016). A bidirectional spectrometer (Figure S1, Table S3) was used to gather Vis–NIR spectra from 0.32–2.55 μm at a sampling interval of 10 nm (under ambient environmental conditions) and an FT-IR spectrometer was used for 2–25 μm at a sampling interval of 4 cm^{-1} (in a dry-air purged environment). In this work we focus solely on the Vis–NIR reflectance spectra, but the FT-IR data are available to interested readers (see Open Research section). Twenty samples were measured: unsorted soil, magnetic–manual separated agglutinates, and magnetic–manual separated non-agglutinates from each of the six samples, as well as manually separated agglutinates and non-agglutinates from soil 62231. The spectra were gathered with an incidence angle of 30° and an emission angle of 0° (i.e., a phase angle of 30°).

For the bidirectional spectrometer measurements, the sample was placed in a black Teflon-coated sample dish that rotated as the measurement was taken, averaging out any rotational asymmetries in the sample. Nearly all measurements were made using a 5 mm diameter sample dish holding ~14–19 mg of sample mass and illuminated by a 9 mm diameter beam (Table S4 and Figure S2). For a few samples, additional measurements were taken in a larger 9 mm diameter dish (Figure S3) or using a narrower 4 mm diameter beam to test whether altering these parameters substantially altered the measured spectra (they generally did not, as described in Text S1 and Figures S4–S8).

Spectra were collected of each sample and of a Spectralon calibration target at the same geometry over four distinct wavelength regions defined by the source lamps and detectors (Table

S3). The ratio of sample measurement to Spectralon measurement was recorded as the sample reflectance spectrum, and the four spectra for the different wavelength regions were stitched together to form a single, continuous spectrum. A correction was then applied to this spectrum to account for Spectralon's nonideal behavior; it is not perfectly reflective at all wavelengths of interest (with absorption bands beyond ~2.14 μm) and it is not a perfectly Lambertian surface (Yang et al., 2019; Bruegge et al., 2001; Zhang et al., 2014).

Although we are primarily interested in how the spectral properties of lunar soils differ by separate type (unsorted, non-agglutinates, agglutinates) and by maturity, the reflectance spectra obtained at RELAB could also be affected by additional factors related to the measurement process: the use of a depolarizer on the illumination source, the size of the sample dish, the width of the illumination beam, and the specific soil particles that end up at the measured sample surface (i.e., sample heterogeneity). We examined each of these factors individually (see details in Text S1) and found that all were small compared to the largest source of variation: sample heterogeneity. Because the volumes of our agglutinate and non-agglutinate separates were small, we typically used a 5 mm dish, and thus the surface area of a soil sample prepared for spectral measurement consisted of a layer of only a few hundred soil particles. We collected spectra of each sample multiple times, with the sample emptied from and returned to the sample cup between each measurement to randomize the soil particles present on the surface. We found that this was the dominant source of variability in the spectra (as seen in the spread in individual spectra in Figure 9).

2.4 Characterizing reflectance spectra

Following conventions used for Moon Mineralogy Mapper (M^3) data (Mustard et al., 2011; Nettles et al., 2011), we characterize the reflectance spectra in terms of their spectral contrast and spectral slope using four parameters: integrated 1 μm band depth, integrated 2 μm band depth, continuum ratio, and albedo (Table 2). We define these parameters in a manner similar to the M^3 analyses, but with adjustments to wavelengths to better match the features in our spectral data.

The 1 and 2 μm integrated band depths are measures of spectral contrast, defined here as

$$IBD_{1\mu m} = \sum_{n=0}^{75} 1 - \frac{R(770 + 10n)}{R_c(770 + 10n)} \quad and \quad IBD_{2\mu m} = \sum_{n=0}^{93} 1 - \frac{R(1570 + 10n)}{R_c(1570 + 10n)}$$

where $R(\lambda)$ refers to reflectance at a given wavelength λ, $R_c(\lambda)$ is the continuum reflectance (defined as a straight line across the absorption band) at wavelength λ, and n is the number of wavelength intervals to be integrated over. Wavelength is specified here by the starting wavelength (770 or 1570 nm) and the wavelength interval of the spectral data (10 nm). In other words, the integrated 1 μm band depth is calculated from spectral data for 770–1520 nm, while the integrated 2 μm band depth is calculated similarly for 1570–2500 nm.

The continuum ratio is a measure of spectral slope and is defined here as R1550/R750 (the ratio of reflectance at 1550 nm and at 750 nm, on either side of the 1 μm band). The albedo

parameter is a measure of overall visible–near-IR brightness and is defined as R1550, since 1550 nm is a wavelength at which the spectral influence of the 1 and 2 μm absorption bands is minimal.

3 Results

3.1 Sorted particles

3.1.1 Agglutinate abundance

We estimate agglutinate abundance as the mass percentage of an agglutinate separate relative to the mass of the soil from which it was separated (i.e., the 125–250 μm size fraction of the given soil) (Figure 4). Note that this metric does *not* account for incorrectly sorted particles within a grain-size separate (Table S2). In comparing these agglutinate abundances to soil maturity (as given by I_S/FeO values from Morris (1978)), mature soils generally have more agglutinates. This is as expected, since agglutinates are a product of the weathering processes that create mature soils. Notably, though, soil 15041 (I_S/FeO = 94; 41% abundance) has a substantially higher agglutinate abundance than the other soils, even compared to the similarly mature soil 62231 (I_S/FeO = 91; 13% abundance).

We also see a notable difference in agglutinate abundance for 62231 between the sample that was separated by the magnetic–manual method (62231.58) versus the sample that was manually separated (62231.52). A comparison of these separation methods is presented in Section 3.1.2, but, in short, this discrepancy in agglutinate abundance is likely due to the lower effectiveness of the manual separation method: the manual separation method results in substantial contamination of the (nominally) agglutinate separate with non-agglutinate particles, and this additional mass artificially inflates the calculated agglutinate abundance (see estimated purity of the agglutinate and non-agglutinate separates in Table S2).

3.1.2 Impact of sorting method (manual vs. magnetic–manual)

We compare the effectiveness of the two sorting methods—manual and magnetic–manual—using microscopic images of the agglutinate separate yielded by each method (Figure 5). Most of the particles in both agglutinate samples show the telltale markers of an agglutinate: irregular shape, vesicularity, a brown color, and a surface texture that varies from rough to glassy, interspersed with mineral fragments. However, we see that not every particle in either separate is an agglutinate, indicating that neither was perfectly sorted.

To quantify how successful each sorting method was, we calculate the sample purity (i.e., the ratio of correctly sorted particles to total particles) by counting the number of agglutinate particles and non-agglutinate particles in microscope images where a representative sample of ~50 particles are present (not shown). We find that the magnetic–manual sorting method yielded a higher-purity 62231 agglutinate separate than the manual method did (95% vs. 75%). We similarly calculate the purity of the 62231 non-agglutinate separates resulting from the two methods and find both to have a purity of about 90%. We also calculate purities for the other samples (all magnetic–manual separated), which yields purities comparable to those for the

399 magnetic–manual separated 62231: on average about 95% agglutinate purity, 85% non-
400 agglutinate purity.
401
402 Based on these observations we conclude that the magnetic–manual method is more
403 effective than the manual method at producing a pure agglutinate separate. Therefore, in the
404 following sections we include only results from the magnetic–manual separated 62231 sample
405 when discussing soil 62231, omitting the manually separated sample data (available in
406 Supplemental Material: Text S2, Figures S9 and S10).
407

408 3.1.3 Variations in agglutinate and non-agglutinate appearance with composition
409 and maturity

410 Four of the agglutinate samples—14259, 62231, 15041, and 79221—have comparable
411 maturity (I_S/FeO values ranging from 81 to 94), but differ in composition (Table 1). As expected
412 based on their iron and titanium content, the non-agglutinate particles are visually distinct based
413 on composition, ranging from an overall brighter appearance for the highland soil to darker for
414 the ilmenite-rich high-Ti mare soil (Figure 6). Although the agglutinates from all of these soils
415 appear morphologically similar, there is also a noticeable darkening of the particles in going
416 from highlands to non-mare to mare soil (Figure 7). Hence, despite vitrification and a large
417 population of opaque npFe, agglutinate appearance and reflectance are not the same from site to
418 site, but depend on local composition.
419
420 There is also a substantial difference in agglutinate appearance across soils 67461, 61141,
421 and 62231 (Figures 8A, 8C, 8E). These soils are similar in composition owing to their shared
422 highlands origin at the Apollo 16 landing site, so differences in appearance are primarily a result
423 of differing maturity: soil 67461 is immature (I_S/FeO = 25), 61141 is submature (I_S/FeO = 56),
424 and 62231 is mature (I_S/FeO = 91). The morphology of the agglutinates is generally comparable
425 across the three soils, but the agglutinates of the immature soil 67461 appear to have a more
426 abundant population of high-reflectance clasts visible at their surface (see Figures 8A vs. 8C and
427 8E). Overall, the agglutinates from the more mature soils 61141 and 62231 are noticeably darker
428 by eye than the agglutinates from the immature soil 67461 (a qualitative observation that is
429 quantified in Section 3.2). The trend of darkening with maturity also holds true for the non-
430 agglutinates from each soil (Figures 8B, 8D, 8F).
431

432 3.2 Vis–NIR reflectance of agglutinates and non-agglutinates

433 Here we compare reflectance properties of the 125–250 μm agglutinate and non-
434 agglutinate separates by examining the reflectance spectra (Figures 9, 10) as well as the
435 calculated spectral parameters defined in Section 2.4 (Table 2, Figure 11). We similarly analyze
436 reflectance spectra of 75–125 μm separates in Section 3.2.3, in which we consider the effects of
437 particle size. Although we calculated four spectral parameters—integrated 1 μm band depth,
438 integrated 2 μm band depth, continuum ratio, and albedo—the two band depth parameters are
439 highly correlated (Table 2). Therefore, we can adequately characterize the spectra with only
440 three parameters, and we omit mention of the integrated 2 μm band depth hereafter.
441

Note that the reflectance of each 125–250 μm unsorted soil, at any given wavelength, should be intermediate to that of the 125–250 μm agglutinate and non-agglutinate separates (since the agglutinate and non-agglutinate separates together constitute the unsorted soil). However, this is only true for two soils: 67461 and 62231. The other four soils have wavelength regions where the mean agglutinate and non-agglutinate spectra are both lower in reflectance than the mean unsorted soil spectrum (Figure 9). As described in Section 2.3 (and discussed in greater detail in Text S1), we explored the causes of variance among spectra collected multiple times of the same sample, and found it was dominantly the result of heterogeneity within a soil and the small number of grains seen by the spectrometer at a time. This was recognized as differences in reflectance when the sample was emptied from and then returned to the sample dish, thereby randomizing which particles were on the surface. In particular, the largest variations were observed for the absolute reflectance of the unsorted and non-agglutinate spectra, which are inherently more heterogeneous (e.g., Figure 2B), whereas the agglutinate spectra were highly consistent (more uniformly dark particles, e.g., Figure 2A). To convey this variance, Figure 9 shows not only the *average* spectrum for each sample, but also the *individual* spectra that constitute each average.

3.2.1 General spectral patterns

While the reflectance spectra of each soil's agglutinate and non-agglutinate components exhibit nuances related to maturity and composition (discussed below), there are general spectral patterns that are present across all six soils. Marked differences in continuum slope, absorption band strength, and albedo distinguish agglutinates and non-agglutinates from each other and from the unsorted soil.

In general, the spectral slope is predicted moreso by the separate type (agglutinate, non-agglutinate, unsorted) than by the composition of the bulk soil (highlands, nonmare, low-Ti mare, high-Ti mare) (Figure S11). For every soil, agglutinates are reddest in spectral slope (continuum ratios of 1.47–1.64), non-agglutinates are bluest (1.11–1.24), and unsorted soils are intermediate (1.13–1.39) (Table 2, Figures 10, 11).

The 1- and 2-μm absorption bands, due to FeO-bearing minerals and glass, also display variations by separate type (Table 2, Figure 11). For each soil, the agglutinates have weaker absorption bands than both the unsorted soil and non-agglutinates, with the integrated 1 μm band depth for agglutinates being on average 25% (13–41%) smaller than for the unsorted soil and on average 41% (23–58%) smaller than for non-agglutinates (Table 2).

For each soil, the albedo parameter is comparable for the non-agglutinate and unsorted separates (Table 2, Figure 10), but lower for the agglutinates: the albedo parameter for agglutinates is on average 19% (10–38%) less than for the unsorted soil and on average 20% (10–38%) less than for non-agglutinates (Table 2). Moreover there is a distinct impact of soil composition on this parameter; it distinguishes the separates of the highlands (Apollo 16) soils from the separates of the nonmare (Apollo 14), low-Ti mare (Apollo 15), and high-Ti mare (Apollo 17) soils, as visually evident in the two-parameter space of albedo vs. integrated 1 μm band depth (Figure 11).

These three parameters—continuum ratio, integrated 1 μm band depth, and albedo—broadly differentiate the reflectance spectra of agglutinates, non-agglutinates, and unsorted soil. Notably, in the two-parameter space of continuum ratio vs. integrated 1 μm band depth, the agglutinate spectra form a cluster distinct from the unsorted and non-agglutinate spectra due to their high continuum ratio (red slope) and small integrated 1 μm band depths (weak absorption bands) (Figure 11). The non-agglutinate and unsorted clusters are not as well-separated, and their overlap is attributable to the effects of soil maturity: the immature 67461 soil has non-agglutinate and unsorted separates that are close together in this space (i.e., they are similar in both continuum ratio and integrated 1 μm band depth).

		Spectral Parameter			
Separate Type	Soil Name	Int. 1 μm Band Depth	Int. 2 μm Band Depth	Continuum Ratio	Albedo
Unsorted	67461	4.45	5.11	1.13	0.29
	61141	3.06	2.17	1.28	0.16
	62231	3.38	2.59	1.18	0.18
	14259	3.75	4.79	1.34	0.10
	15041	4.89	4.91	1.39	0.10
	79221	4.23	3.51	1.33	0.09
	Average	**3.96**	**3.85**	**1.27**	**0.15**
Non-agglutinates	67461	4.32	5.55	1.11	0.29
	61141	3.61	2.91	1.19	0.16
	62231	3.47	3.04	1.13	0.19
	14259	4.91	7.18	1.22	0.10
	15041	10.07	10.88	1.24	0.10
	79221	6.54	5.59	1.23	0.09
	Average	**5.49**	**5.86**	**1.19**	**0.15**
Agglutinates	67461	3.31	1.74	1.55	0.18
	61141	2.42	0.88	1.64	0.14
	62231	1.99	0.76	1.55	0.14
	14259	3.28	2.49	1.60	0.09
	15041	4.25	3.59	1.47	0.08
	79221	2.80	1.41	1.56	0.08
	Average	**3.01**	**1.81**	**1.56**	**0.12**

Table 2. Spectral parameters calculated for the mean reflectance spectra of the 125–250 μm unsorted, non-agglutinate, and agglutinate separates. Integrated band depths are defined over 770–1520 nm (for the 1 μm band) and 1570–2500 nm (for the 2 μm band). Continuum ratio is

defined as R1550/R750. Albedo is R1550. See Section 2.4 for more detailed definitions of these parameters.

3.2.2 Effects of varying maturity

The three Apollo 16 soils have similar highlands composition (Taylor et al., 2010) and thus their spectral differences (Figure 12) are largely attributable to variations in maturity. Namely, we see notable differences in albedo and absorption band strength—and minor differences in continuum slope—that set the immature soil (67461) separates apart from those of the submature (61141) and mature (62231) soils. While previous studies have presented similar results to those detailed below for unsorted soils (e.g., Taylor et al., 2001a, 2010; Noble et al., 2001) here we also explore the spectral changes related to maturity for the non-agglutinate and agglutinate separates, as well as their relative spectral contributions to the unsorted soil.

The spectrum for each immature separate has a higher albedo than the corresponding submature and mature separate (Figure 11, Figure 12 left), which aligns with the visually brighter appearance of the immature particles (Figure 8). This higher albedo is most striking for the unsorted soils (albedo parameter of 0.29 for immature vs. 0.16 for submature and 0.18 for mature) and for the non-agglutinates (0.29 vs. 0.16 and 0.19), and evident to a lesser extent for the agglutinates (0.18 vs. 0.14 and 0.14) (Table 2). Agglutinates are thus low in albedo regardless of the level of maturity of the associated soil, but the albedo of non-agglutinate separates decreases substantially from immature to mature. We note that for the non-agglutinates, it appears that there is a larger fraction of moderate-albedo breccia fragments in the submature and mature samples than in the immature sample (Figure 8). These dark, glassy melt breccias were of higher abundance in the moderately magnetic particles of each sample (Figures 3B, 3E).

For each separate type (i.e., unsorted, non-agglutinates, agglutinates), the absorption bands are stronger (i.e., the integrated 1 μm band depth is greater) for the immature sample than for the submature and mature samples (Figures 11, 12). For the unsorted separates, the immature sample's integrated 1 μm band depth is 45% greater than for the submature sample and 32% greater than for the mature sample. For the non-agglutinates these band depth differences are more modest, with the immature sample's band depth being 20% and 25% greater than for the submature and mature samples, respectively. For the agglutinates these band depth differences are much larger, with the immature sample's band depth being 37% and 67% greater than for the submature and mature samples, respectively.

The continuum slope shows the smallest differences attributable to maturity (Figures 11, 12). For the unsorted separates, the immature sample's continuum ratio is 12% less than for the submature sample and 4% less than for the mature sample. For the non-agglutinates these continuum ratio differences are smaller, with the immature sample's band depth being 7% and 2% less than for the submature and mature samples, respectively. For the agglutinates these continuum ratio differences are even smaller, with the immature sample's continuum ratio being 6% and 0% less than for the submature and mature samples, respectively. Thus, while the agglutinates overall have a substantially redder slope than the non-agglutinates, this red slope is largely consistent among immature, submature, and mature agglutinates.

546 For the submature (61141) soil, we observe a peculiarity in the spectra. One might expect
547 the submature separates to have spectral characteristics intermediate to those of the immature
548 and mature soil separates. Yet the spectra for the submature separates have steeper continuum
549 slopes and lower albedos than the corresponding spectra for the immature and mature soils (one
550 exception: the submature agglutinates have an albedo comparable to that of the mature
551 agglutinates). These results for the submature soil are in contrast to expectations based on
552 maturity, but they are congruent with the spectral measurements of Taylor et al. (2010), who
553 observed spectra of some size fractions of submature soil 61141 to be lower in reflectance than
554 the corresponding spectra of the more mature soil 62231 (unlike spectra of another submature
555 soil (67481) and another mature soil (64801), which were higher in reflectance than the
556 corresponding spectra of 62231; see Figure 5 in Taylor et al., 2010). Given these observations,
557 the unexpected spectral properties of soil 61141 seem to be characteristic of that soil itself (rather
558 than being representative of submature agglutinates, non-agglutinates, or unsorted soil in
559 general). Therefore the spectral differences we observe between separates of submature soil
560 61141 and of mature soil 62231 do not necessarily have broader implications for how the
561 spectral properties of agglutinates and non-agglutinates change as a given soil matures.
562

563 3.2.3 Effects of particle size

564 For sample 62231, we explored one additional variable: particle size. Differences in
565 particle size are associated with changes in composition and reflectance (e.g., Taylor et al.,
566 2001a, 2001b, 2010; Noble et al., 2001), and the reflectance spectra of smaller particle size
567 separates (i.e., 10–20 and 20–45 μm) tend to be most similar to the bulk soil (Pieters et al., 1993;
568 Fischer, 1995). This motivates an analysis of spectral properties for smaller particle sizes, but our
569 magnetic–manual method of concentrating agglutinates is only practical for particle sizes larger
570 than ~125 μm, as smaller particles cling to tweezers and other tools. Thus we performed a
571 magnetic-only separation on the 75–125 μm size fraction of sample 62231. Unfortunately,
572 without changes to procedure (e.g., using the ethanol-filled pipette method of Adams and
573 McCord (1973), as described in Section 2.2), magnetic separation of even smaller size fractions
574 is not feasible—particles cling to the magnetic separator and do not flow easily down its chute.
575
576 The magnetic separation yielded three distinct 75–125 μm separates: the agglutinate-
577 rich/highly magnetic particles (hereafter referred to as *aggl-rich (high-mag)*), the low-
578 agglutinate/moderately magnetic particles (*low-aggl (mid-mag)*) and the no agglutinate/least
579 magnetic particles (*no aggl (low-mag)*) (Figure 3). Recall that these same three separates were
580 yielded by magnetic separation of the larger 125–250 μm size fraction as well, but in that case
581 we combined the low-aggl (mid-mag) and no aggl (low-mag) separates and then manually sorted
582 them into the agglutinate and non-agglutinate categories. In contrast, for the 75–125 μm size
583 fraction we have no subsequent manual separation, so we retained the three magnetic groups.
584 This discrepancy complicates direct comparisons between the 75–125 μm and 125–250 μm
585 separates, but we can still draw some comparisons, as follows.
586
587 The 75–125 μm aggl-rich (high-mag) separate is comparable to the 125–250 μm
588 agglutinate separate, but has lower purity of agglutinates: it is missing some less-magnetic
589 agglutinates and includes some highly magnetic non-agglutinates. Yet when we consider the
590 spectra for these separates (the dotted yellow and dotted dark yellow spectra in Figure 13), we

find that they are almost identical in both absolute and normalized reflectance, despite the differences in particle size and purity between these samples. We might have expected the 75–125 μm agglutinates to have higher reflectance than the 125–250 μm agglutinates based on their smaller particle size as well as their lower purity (i.e., a higher percentage of the brighter non-agglutinate particles).

The 75–125 μm low-aggl (mid-mag) and no aggl (low-mag) separates (dashed medium blue and light blue spectra in Figure 13), if mixed together, would be most comparable to the 125–250 μm non-agglutinate separate (dashed dark blue). However this mixture would have lower purity of non-agglutinates, as it would be missing highly magnetic non-agglutinates and would include some less magnetic agglutinates. When we consider the spectra for these separates, we find that the 75–125 μm low-aggl (mid-mag) is similar in absolute reflectance to the 125–250 μm non-agglutinates, albeit with lower reflectance at wavelengths shorter than 2.0 μm. Meanwhile the 75–125 μm no-aggl (low-mag) absolute reflectance is far greater at all wavelengths than for all of the other separates. The normalized reflectance spectra show a different pattern, where the 75–125 μm no-aggl (low-mag) separate and the 125–250 μm non-agglutinates have a similar slope (that is also similar to the 125–250 μm unsorted soil), while the 75–125 μm low-aggl (mid–mag) has a redder slope (similar to the 75–125 μm unsorted soil).

Looking to the unsorted soil spectra (solid gray and black spectra in Figure 13), we see that the 75–125 μm spectrum is almost identical to the 125–250 μm spectrum at the UV and visible wavelengths, but has higher reflectance and a redder slope in the near-infrared. This matches the spectral patterns observed for the same size fractions of soil 10084 by Pieters et al. (1993).

4 Discussion

4.1 Defining an agglutinate

Agglutinates constitute a key component of lunar soils, both in terms of abundance (in mature soils) as well as spectral impact. Yet there is ambiguity in how the literature defines what is and isn't an agglutinate. Here we discuss the nuances of defining an agglutinate and how differing definitions of agglutinates impact comparison of our results to those of prior agglutinate work.

In an abstract, conceptual sense, agglutinates are agglomerates of mineral and lithic fragments bound together by impact-generated glass. However in practice it is challenging to distinguish individual soil particles as agglutinate or non-agglutinate. For example, is a particle still an agglutinate if it contains a minimal, but nonzero amount of agglutinitic glass? Should the distribution of the glass within the particle also be considered (e.g., if the particle is composed of an agglutinitic glass-rich half fused with a glass-free mineral fragment half)? There is no clear agreement on this matter, with the literature of agglutinate analyses using a myriad of definitions of an agglutinate.

Some studies, as ours, have identified agglutinate particles on the basis of visual appearance (McKay et al., 1972; Heiken & McKay, 1974; Basu et al., 1982). This approach is

effective for particles that are clearly agglutinate or non-agglutinate, but relies on the judgment of the observer for the numerous cases that are difficult to classify (e.g., distinguishing agglutinates from dark, glassy melt breccias). In our study an additional element of variance is introduced to visual identification by our preprocessing step (i.e., our magnetic separation step that concentrated agglutinates), as one's perception of whether a given particle is or isn't an agglutinate may be influenced by characteristics of the surrounding particles (e.g., one's threshold for "agglutinate" may be more stringent when the sample's particles are difficult to categorize and require a high level of scrutiny). In contrast to the visual identification approach, other studies have used quantitative definitions based on particle chemistry and morphology (Simon & Papike, 1981; Taylor et al., 1996, 2001a, 2010). For example, in Taylor et al.'s study of the 90–150 μm size fraction of mare soils, agglutinates were defined as particles with 30–80% Al-rich glass and >100 μm^2 total void (vesicle) area (Taylor et al., 1996).

Further complicating any definition of agglutinates is their evolution over time. Exposure of surface soils to space weathering processes not only increases agglutinate abundance, but also alters the composition, spectral properties, and appearance of the agglutinates themselves. We observed this phenomenon in the Apollo 16 soils of varying maturity, with the agglutinate grains from more mature soils being significantly darker in appearance owing to their higher iron metal content. However these observations were only for Apollo 16 (highlands) soils, so what remains to be seen is how this evolution path of maturing agglutinates varies according to the composition of the bulk soil.

The soils studied here were chosen because they have been characterized by previous studies in terms of mineralogy, chemistry, maturity, and spectral properties (Taylor et al. 1996, 2001a, 2001b, 2010; Basu et al., 1982; McKay et al., 1972; Heiken & McKay, 1974; Simon & Papike, 1981; Morris, 1978; Pieters et al., 2002). By comparing our agglutinate abundance results to those of prior studies (Figure 14), which differ in agglutinate definitions, we can assess how this ambiguity in defining agglutinates can impact measurements of their abundance. For the soils we studied, we calculated agglutinate abundance as a weight percentage based on the masses of the agglutinate and non-agglutinate separates. McKay et al. (1972), Heiken and McKay (1974), and Basu et al. (1982) counted the percentage of agglutinate particles. Simon and Papike (1981) and Taylor et al. (1996) gathered modal abundance (i.e., a volume percentage) of agglutinate particles. The Lunar Soil Characterization Consortium (Taylor et al., 2001a, 2010) also gathered modal abundance, but agglutinitic glass was distinguished based on its chemistry at the sub-particle level (glass within an agglutinate was included and mineral fragments within an agglutinate were excluded, rather than categorizing whole particles as agglutinate or non-agglutinate); impact glasses were also lumped with agglutinitic glass.

Yet despite these differences in how agglutinate abundance is measured, we see a fairly consistent overall trend of decreasing abundance for larger size fractions (barring the data for soil 15041 from Basu et al. (1982), where there isn't a clear correspondence between agglutinate abundance and particle size). Our agglutinate abundance results for the 125–250 μm soils match this trend, but are noticeably on the low end of agglutinate abundance. These low values may indicate a difference in particle mass density between agglutinates and non-agglutinates, as we measured abundance based on mass whereas others used the number or volume of agglutinate particles. Another possible cause may be differences across studies in how often non-agglutinate

particles were incorrectly counted as agglutinates and vice versa (particularly when there are similarities in visual appearance and magnetic properties, as for dark, glassy melt breccias).

4.2 New insights into agglutinate reflectance spectra

The agglutinate spectra presented here provide new insights into the spectral variability of agglutinates with respect to soil composition and maturity. These soil characteristics appear to control spectral albedo and band depth (Figure 11). In terms of albedo—measured here as 1550 nm reflectance—the Apollo 16 (highlands) agglutinate spectra are all higher in albedo than the Apollo 14 (non-mare), 15 (low-Ti mare), and 17 (high-Ti mare) agglutinate spectra. Furthermore, among the Apollo 16 agglutinate spectra, albedo (and band depth) decreases with increasing soil maturity. However, albedo and band depth do not distinctly separate the agglutinate spectra from the non-agglutinate and unsorted spectra; there is overlap in the range of these parameter values for the agglutinate spectra versus for non-agglutinate and unsorted spectra.

The patterns in albedo and band depth highlight the complexity of agglutinate spectral properties and can inform future spectral modeling of lunar soils, an area in which agglutinates have historically been modeled simplistically for lack of comprehensive spectral data. For example, some work has simply treated agglutinates as glass, ignoring the effects of their npFe (e.g., Warell & Davidsson, 2010). Some have used the agglutinate spectrum of Pieters et al. (1993) as representative of all agglutinates, despite its high-titanium mare composition (e.g., Li & Li, 2011). Many efforts have used empirical parameters to represent agglutinates (Shkuratov et al., 1999; Clark et al., 2001; Hapke, 2001; Poulet et al., 2002; Poulet & Erard, 2004; Lawrence & Lucey, 2007; Denevi et al., 2008; Nimura et al., 2008). This current work has shown, though, that agglutinate spectra vary substantially across soils of different bulk composition, highlighting that the bulk soil properties must be taken into account for accurate spectral modeling of agglutinates.

Moreover, agglutinate spectra vary with maturity—at least for the specific immature, submature, and mature soils of this study—suggesting the existence of an agglutinate "life cycle" over which its spectral properties change due to progressive weathering (more specifically due to changes in npFe, such as the increasing npFe abundance indicated by increasing I_S/FeO values of the bulk soil). However, since the soils of different maturities studied here were all (Apollo 16) highlands soils, we cannot yet surmise how this agglutinate life cycle might vary across soils of different composition—will non-highlands agglutinates show different maturing trends, perhaps due to differences in the bulk soil's iron abundance? It may also be enlightening to study other highland soils to better characterize the robustness of these maturing trends (particularly since the submature soil 61141's properties may be atypical, such as having a lower albedo than the more mature soil 62231). These are areas for future investigation via study of other immature and submature lunar soils.

A parameter in which the agglutinate spectra *are* generally comparable is spectral slope—quantified in this work as the continuum ratio of 1550 nm reflectance to 750 nm reflectance. Unlike albedo and band depth, this continuum ratio distinctly separates the

agglutinate spectra from the non-agglutinate and unsorted spectra, which all have smaller continuum ratios (Figure 11).

The spectral slopes of the agglutinate spectra also provide new insight into a question that has persisted in the literature of lunar soils: what causes the characteristic spectral changes (darkening and reddening) of maturing soils? Historically these changes have primarily been attributed to two sources—agglutinates and depositional rims—both of which form and accumulate in the lunar soil as it is exposed to space weathering processes. Agglutinates are typically considered to darken rather than redden the unsorted spectra due to the large npFe within agglutinate particles (e.g., Britt & Pieters, 1994; Keller et al., 1998; Noble et al., 2007; Pieters & Noble, 2016). Meanwhile, reddening is typically attributed to the small npFe found in the rims of all weathered particles (both agglutinates and non-agglutinates) (e.g., Hapke, 1973; Hapke et al., 1975; Cassidy & Hapke, 1975; Hapke, 2001; Pieters et al., 1993). Yet the agglutinate spectra in this study are all quite steep (red) in slope (Figure 10), suggesting that it is the agglutinates (and potentially their depositional rims), rather than the npFe-rich rims of non-agglutinates, that primarily contribute to reddening of the unsorted soil spectra. These results reframe our understanding of the relative spectral roles of agglutinates and rims: agglutinates play a greater role in weathering-associated spectral reddening than previously thought.

Admittedly we cannot isolate this reddening impact of agglutinates with further granularity—to what extent are these spectral effects attributable to an agglutinate grain's own depositional rim versus its interior? Given that rims can vary in microstructure and chemistry (Keller & McKay, 1997), it is conceivable that the depositional rims that form on agglutinates are fundamentally different from those that form on non-agglutinates, leading to spectral reddening that is attributable to the agglutinate component of the soil, but is driven specifically by the rims of the agglutinates.

To better understand why agglutinates have such steep spectral slopes despite the large sizes of npFe grains within them, we compared the agglutinate and non-agglutinate spectra to spectra of npFe in silica gel from Noble et al. (2007). These npFe spectra represent a range of average npFe sizes (8 nm, 15 nm, 35 nm, and 40 nm) and weight percentage abundances. Here we consider only the normalized spectra, focusing on how well the agglutinate and non-agglutinate spectra match the npFe spectra in terms of spectral slope (Figure 15).

The closest spectral matches for both agglutinates and non-agglutinates are npFe with average sizes of 15 nm and 35 nm. However, npFe abundance is a critical parameter in fitting the spectra as well. The agglutinate and ~15 nm npFe spectra match best for npFe abundance of about 0.13 wt%. For matching the agglutinate and ~35 nm npFe spectra, neither the 0.02 wt% nor the 0.20 wt% spectra are truly good fits, with the former being too shallow in slope and the latter too steep. Therefore one might expect an intermediate abundance (between 0.02 wt% and 0.20 wt%) of ~35 nm npFe to produce a spectrum that fits the continuum slopes of the agglutinate spectra. In contrast the non-agglutinate spectra are fit best by smaller abundances of ~15 and ~35 nm npFe (about 0.07 wt% and 0.02 wt%, respectively) (Figure 15). These spectral comparisons suggest similar average npFe sizes within both the agglutinates and non-agglutinates, but greater npFe abundance in the agglutinates. Given that increasing npFe

abundance in silica gel yields a steeper spectral slope (Figure 15), the abundance of npFe appears to play a key role in causing the steep spectral slope of agglutinates.

An important caveat here is that this spectral comparison does not provide a constraint on the *size distribution* of npFe within agglutinates, which can also have a spectral impact (e.g., Lucey & Riner, 2011). The range of npFe sizes can be quite wide for agglutinates—larger npFe is typically found within the agglutinate particle interior, while smaller npFe spherules occur in the particle rims. James et al. (2002) estimated an average npFe size within agglutinates of 120 nm with a standard deviation of 20 nm, while Keller and Clemett (2001) estimated an average npFe size of 3 nm in the depositional rims (of all lunar soil particles, not only agglutinates). However these estimates themselves have uncertainties; the scanning electron microscopy used by James et al. is limited in its ability to resolve—and therefore tends to underestimate—the smallest sizes of npFe (<10 nm), while the transmission electron microscopy used by Keller and Clemett images smaller spatial areas and therefore has greater difficulty sampling a representative number of particles (sampling ~1300 npFe particles compared to the ~9600 of James et al.).

These spectral comparisons motivate future work on the spectral impact of npFe within agglutinates. While npFe size is an important parameter, npFe abundance plays a prominent role as well. Moreover, Arnaut et al. (2021) found that the density and distribution of npFe particles, rather than just their size or abundance, may have distinct effects on spectral slope due to interparticle interactions when the npFe particles are arranged in layers or clusters. The spectral impact of npFe is complex, with nuances that have yet to be fully understood. Future work analyzing SEM and TEM image data of individual agglutinate grains can elucidate this matter.

4.3 Contribution of agglutinates to bulk reflectance spectra

Our new insights into the spectral properties of agglutinates come with an important caveat: they only strictly hold for the 125–250 μm size fraction that we studied. However for applications such as spectral modeling of lunar soils, one would rather understand agglutinate spectral signatures as they exist in situ, across a range of size fractions and mixed within the bulk soil. Therefore we still have two lingering questions: (1) how well do the 125–250 μm size fraction spectra (investigated in this study) represent the spectral properties of bulk agglutinates (across size fractions), and (2) how well does spectral mixing of agglutinates and non-agglutinates in the 125–250 μm size fraction translate to the same spectral mixing in the bulk soil? While definitively answering these questions will require further study, here we discuss what we know based on the findings of this study and the existing literature.

First, we consider how bulk agglutinate spectra may compare to the 125–250 μm agglutinate spectra gathered in this study. Recall that the 125–250 μm size fraction was chosen for this study owing to practical considerations (feasibility of manual separation) rather than any particular spectral relevance. In fact, Fischer (1995) found smaller particle size separates (10–20 and 20–45 μm)—rather than larger size fractions like 125–250 μm—to be most spectrally similar to the bulk (<1 mm) soil. If this pattern holds true within the agglutinate portion of the soil as well, one expects smaller agglutinates to better represent the spectral properties of agglutinates as a whole.

This spectral dominance of smaller size fractions motivated our analysis of the 75–125 μm size fraction of soil 62231, which aimed to identify patterns of spectral changes as particle size decreases (Section 3.2.3). Although comparisons between the 75–125 μm and 125–250 μm size fractions are complicated by their different separation methods—the former magnetic-only and the latter magnetic–manual—our results suggest that agglutinates for the two size fractions are spectrally quite similar.

Given the spectral similarity between the 75–125 μm and 125–250 μm agglutinates, can we assume similar agglutinate spectra for smaller size fractions? Our evidence from just two size fractions seems too limited to draw any strong conclusions. However there is some evidence that agglutinates of varying size fractions are at least similar in composition (per the findings of Taylor et al. (2001a, 2001b, 2010) that agglutinitic glass composition is relatively invariant to particle size across the <10 μm, 10–20 μm, and 20–45 μm size fractions). Yet even if agglutinate composition (and associated spectral properties) is invariant to particle size, the particle size itself will influence the spectrum (i.e., smaller particles tend to have higher reflectance).

Second, let's consider how spectral mixing of agglutinates and non-agglutinates might differ for the bulk soil versus for the 125–250 μm size fraction. We get some insight into this from our analysis of the 75–125 μm and 125–250 μm size fractions of soil 62231. For these two size fractions, the unsorted soil spectra are comparable at visible wavelengths, but diverge at longer wavelengths due to the 75–125 μm spectrum's redder near-IR slope (Figure 13). This redder slope in the smaller size fraction may be due to increased agglutinate abundance (as this abundance tends to increase for smaller size fractions; Figure 14). If so, we would expect the unsorted soil spectra for even smaller size fractions to be comparable to our unsorted spectra at visible wavelengths, but even redder at longer (near-IR) wavelengths. We would then expect similar of the bulk soil spectra, since smaller size fractions best spectrally represent the bulk.

Striking, though, is how closely the 75–125 μm unsorted spectrum is tracked by the spectrum of the low-aggl (mid-mag) separate (Figure 13). This separate consists of moderately magnetic particles, including many dark, glassy melt breccias and a very small number of agglutinates (Figures 3B, 3E). We did not consider this separate in our other analyses, where all non-agglutinates were lumped together, yet it appears that these moderately magnetic particles may warrant further study as an important contributor to the unsorted soil spectrum.

The highly influential work of Pieters et al. (1993) also considered the relative contributions of agglutinates and space-weathered rims to the bulk spectra of weathered soils. In that work, agglutinates were also separated from two size fractions (250–500 μm and >500 μm) of sample 10084. The spectra of these agglutinates were compared to spectra of the <250 μm fraction of bulk soil and smaller size fractions, and the fact that these agglutinates were not as red was interpreted to mean that the agglutinates were not the cause of the bulk soil's red spectral slope. However, the 250–500 μm agglutinates were redder than the >500 μm agglutinates, and these agglutinates were not compared to like size fractions.

To test whether the finest fraction of soils (<25 μm) was strongly affected by agglutinates, Pieters et al. measured the reflectance spectrum of an unsorted 45–75 μm size

separate from an agglutinate-rich soil, ground down to a size of <25 μm, and found that it was too bright and its slope was shallower compared to the <25 μm soil fraction. This spectral difference was attributed to the physical difference in the ground sample: its particles had exposed interiors, minimizing the spectral impact of the particle rims. This result, combined with other work suggesting that agglutinate abundance decreases with decreasing particle size (Labotka et al., 1980; Simon et al., 1981), led to the argument that the rims of soil grains in the finest fraction are responsible for the spectral changes associated with space weathering, rather than agglutinates. However, grinding would expose fresh mineral fragments from within the agglutinates, in which glass constitutes only ~30% of the non-vesicle area (Baker et al., 2020). Thus, this ground soil is likely not an appropriate test of the nature of the spectral properties of the finest fraction of agglutinates. Moreover, since that time we now know that agglutinates increase in abundance with decreasing particle size rather than decrease (Figure 14 and references therein), and now, we also know that agglutinates cause spectral reddening. Thus, agglutinates may indeed play an important role in defining the spectra of the finest fraction of soils, and the relative contributions of space-weathered rims and agglutinates to the overall bulk spectra of mature soils remains an important open question.

These questions regarding the in situ spectral signature of agglutinates could be clarified with further work on separating smaller size fractions of agglutinates. However this would require a different agglutinate/non-agglutinate separation methodology than the one presented here, as we noted that the fine particles (<75 μm) do not easily flow down the magnetic separator chute used in our method. An alternative method that may work for such fine particles is described by Adams and McCord (1973), wherein soil was passed through a column of ethanol attached to a magnetic separator, yielding agglutinate separates from a <250 μm lunar soil sample. Yet, as described in Section 2.2, this method has its own unique challenges to overcome, including the unintended separation of highly magnetic non-agglutinates alongside the agglutinates.

4.4 Unaddressed questions on non-agglutinates

This work's primary focus has been on the agglutinate portion of lunar soils. To simplify discussion we have referred to the remainder of the soil as the "non-agglutinates", but this catch-all term belies the heterogeneity of these particles and their resulting spectral complexities—itself a valuable topic of study for better understanding the reflectance spectra of bulk lunar soils. Although a thorough spectral characterization of the many types of non-agglutinates is beyond the scope of this work, our findings provide insights into and provoke questions on this subject that we broach here as a starting point for future work.

In particular, questions arise from the soil separates we obtained from magnetically separating the 75–125 μm size fraction of the mature soil 62231 (Figure 3). The no aggl (low-mag) separate is far brighter than the unsorted soil it was derived from (Figures 3A, 13), which suggests that, if the particles in this separate have space-weathered rims, these rims do not have a strong spectral impact on the bulk soil. On the other hand the low-aggl (mid-mag) separate is much darker (Figures 3B, 13) and is spectrally similar to the unsorted soil (Figure 13). What makes these two separates—both primarily consisting of non-agglutinates—so visually distinct?

What are the features of the non-agglutinate particles in the low-aggl (mid-mag) separate that make it so dark in appearance?

Whereas the no aggl (low-mag) particles are largely homogeneous, each composed of uniformly high-reflectance mineral fragments (Figures 3A, 3D), the low-aggl (mid-mag) particles appear to contain a large population of more heterogeneous particles—dark, glassy melt breccias—that are intermediate in reflectance (Figures 3B, 3E). In our manual separation, most of these particles would not have been included as agglutinates because they have more angular margins and less glassy texture (see Figure 7). Further study of this population of particles within the low-aggl (mid-mag) separate is needed to determine the nature of their low reflectance and their significance for understanding space weathering processes. Characterizing the spectral properties of these particles and the abundance and nature of their npFe could provide greater insight into how regolith evolves as it is weathered.

5 Conclusions

By isolating and characterizing agglutinates from a suite of lunar soils, we aimed to develop a comprehensive understanding of agglutinate properties across the lunar surface. The six soils in the suite represent the diversity of the sampled sites, spanning both a range of soil compositions (highlands 62231, non-mare 14259, low-Ti mare 15041, high-Ti mare 79221) and of soil maturities (immature 67461, submature 61141, mature 62231). While we primarily studied the 125–250 μm size fraction of these soils, we have also considered the impact of particle size by characterizing 62231 agglutinates from the 75–125 μm size fraction as well.

Regarding methodology, we find that separating out 125–250 μm agglutinates is most effective using a two-step magnetic–manual separation technique rather than either magnetic separation or manual separation alone. This magnetic–manual method yielded sample purities of ~95% for agglutinate separates and ~85% for non-agglutinate separates. However the manual part of this method makes it both time-intensive and limited to large particles; magnetic separation alone may still be the more appropriate method for some applications, such as investigations of fine (<125 μm) particles, and there is certainly still unexplored potential for improving the magnetic separation method (e.g., by optimizing the magnetic separator settings).

Notably, the reflectance spectra of the agglutinate/non-agglutinate separates and the unsorted soil show similar spectral patterns across all six soils: for each soil the agglutinate spectrum is redder in slope than the unsorted spectrum from the same soil while the non-agglutinate spectrum has a shallower (bluer) slope. Additionally, each agglutinate spectrum is lower in overall reflectance and has weaker absorption bands than the corresponding non-agglutinate and unsorted soil spectra. The consistent pattern in spectral slope is particularly intriguing, suggesting that it is the agglutinates (rather than the non-agglutinates) that contribute to reddening of the unsorted soil—at least for the studied size fractions of 125–250 μm and 75–125 μm.

Among the Apollo 16 soils of varying maturity, we find that the agglutinates from the immature soil are noticeably higher in reflectance and have weaker absorption bands than the agglutinates from submature and mature soils, but they do not differ substantially in spectral

slope. This novel finding suggests the existence of an agglutinate "life cycle"; the weathering of a lunar soil entails not only an increase in agglutinate abundance, but also alteration of the physical and spectral properties of said agglutinates.

The npFe within weathered rims of soil grains and agglutinates is generally considered the driver of reddening and darkening of lunar soils, with smaller npFe (<10 nm) primarily reddening and larger npFe (>40 nm) primarily darkening (Noble et al., 2007). Based on comparison to spectra of npFe in silica gel from Noble et al. (2007), we find that the *abundance* of npFe may be particularly relevant as well for agglutinate-associated reddening, with the best spectral matches between agglutinates and npFe being at higher npFe abundances than the best matches between non-agglutinates and npFe. However this analysis does not constrain the distribution of npFe sizes within each agglutinate particle. Future studies of the agglutinate separates may provide a more robust estimate of npFe abundance and size distribution, providing greater context for the agglutinate spectral characterization presented in this study.

Our work here begins to illustrate the spectral complexities of lunar agglutinates. In particular, our findings suggest that agglutinates play a different spectral role in the weathering of lunar soils than previously thought, contributing not only to the darkening of mature soils, but also to their reddening. Yet there is still much to be done to comprehensively characterize the spectral properties of lunar agglutinates, and numerous avenues of future work are motivated by the myriad questions that remain. For instance, how might agglutinate spectra differ across grain size fractions, beyond the 125–250 μm size fraction that we primarily focused on in this study (and particularly for the smaller size fractions that may better represent the spectral properties of the bulk soil)? How do agglutinate and non-agglutinate particles spectrally mix, and how do non-linearities in this mixing process impact the spectrum of the bulk soil? And, complicating the debate on the spectral role of agglutinates versus the space-weathered rims on soil grains, to what extent can the spectral properties of agglutinates be attributed to space-weathered rims on the agglutinate grains themselves? Perhaps these questions and more will be answered by future studies of lunar agglutinates, further refining our understanding of the lunar surface and its weathering over time.

Acknowledgments

We thank Ben Wing, Karen Stockstill-Cahill, and Karl Hibbitts (Johns Hopkins University Applied Physics Laboratory) for initial assistance with spectral characterization of the lunar soil samples. We also thank the two reviewers Tim Glotch and Bruce Hapke, as well as Carle Pieters and Michelle Thompson, for thoughtful feedback that improved the manuscript.
This work was primarily funded by NASA LDAP grant 80NSSC17K0418 to co-author BWD. The contributions of co-authors ALG, MLZ, and LMB were facilitated by the ASPIRE program (APL's Student Program to Inspire, Relate, and Enrich).
RELAB is a multiuser facility supported by NASA grants.

Open Research

Materials used in and produced by this work can be located as follows.

Soil samples:
Apollo lunar soils were obtained from the NASA Johnson Space Center. The sample IDs for the soils are: 67461.168, 67461.45, 61141.5, 62231.52, 62231.58, 14259.136, 15041.47, 79221.158.

Reflectance spectra:
All spectral data gathered for this study (of agglutinate/non-agglutinate separates and of unsorted soils) can be downloaded from the RELAB Spectral Database within the PDS Geosciences Node Spectral Library (https://pds-speclib.rsl.wustl.edu/search.aspx?catalog=RELAB). The Specimen IDs are LS-BWD-**[xxx]**, where **[xxx]** ranges from 140–165 (e.g., LS-BWD-140).
These spectra are also available directly from the RELAB Spectral Database (https://sites.brown.edu/relab/relab-spectral-database/).

The spectra of nanophase iron in silica gel from Noble et al. (2007) can be downloaded from the RELAB Spectral Database within the PDS Geosciences Node Spectral Library (https://pds-speclib.rsl.wustl.edu/search.aspx?catalog=RELAB). The Specimen IDs are SN-CMP-**[xxx]**, where **[xxx]** is 016, 019, 021, 023, 027, 032, 037–040, 045–050, 054–060, 062, 064, 066, 068, 069, 074–129, 139–145 (e.g., SN-CMP-016). Note that in this study we plotted the silica gel spectra measured over 300–2600 nm (rather than the 300–880 nm spectra that are also found under the same Specimen IDs).
These spectra are also available directly from the RELAB Spectral Database (https://sites.brown.edu/relab/relab-spectral-database/).

Software:
Microscope images were edited (contrast stretching for Figure 1; white balancing for Figures 2, 5–8) and all figures were formatted using Adobe Photoshop.
Data analysis and plotting were done using Python v3.9.16 (Python Software Foundation, 2022) with additional packages matplotlib v3.7.1 (Hunter, 2007), pandas v1.5.3 (The pandas development team, 2023), numpy v1.23.5 (Harris et al., 2020), and tabulate v0.8.10 (Astanin, 2022).

References

Adams, J. B., & Charette, M. P. (1975). Effects of maturation on the reflectance of the lunar regolith: Apollo 16 — A case study. *The Moon*, *13*(1), 293–299. https://doi.org/10.1007/BF00567521

Adams, J. B., & McCord, T. B. (1970). Remote sensing of lunar surface mineralogy: Implications from visible and near-infrared reflectivity of Apollo 11 samples. In *Geochimica et Cosmochimica Acta Supplement, Volume 1. Proceedings of the Apollo 11 Lunar Science Conference held 5-8 January, 1970 in Houston, TX. Volume 3: Physical Properties. Edited by AA Levinson. New York: Pergamon Press, 1970., p. 1937* (Vol. 1, p. 1937).

Adams, J. B., & McCord, T. B. (1971a). Alteration of Lunar Optical Properties: Age and Composition Effects. *Science*, *171*(3971), 567–571. https://doi.org/10.1126/science.171.3971.567

Adams, J. B., & McCord, T. B. (1971b). Optical properties of mineral separates, glass, and anorthositic fragments from Apollo mare samples. In *Lunar and Planetary Science Conference Proceedings* (Vol. 2, p. 2183).

Adams, J. B., & McCord, T. B. (1973). Vitrification darkening in the lunar highlands and identification of Descartes material at the Apollo 16 site. In *Lunar and Planetary Science Conference Proceedings* (Vol. 4, p. 163).

Arnaut, M., Wohlfarth, K., & Wöhler, C. (2021). The interaction between multiple nanophase iron particles changes the slope of lunar reflectance spectra. Presented at the EPSC2021, Copernicus Meetings. https://doi.org/10.5194/epsc2021-770

1058 Astanin, S. (2022, June 21). Tabulate (Version 0.8.10) [OS Independent]. Retrieved from
1059 https://github.com/astanin/python-tabulate
1060 Baker, A. E., Jolliff, B. L., Carpenter, P., Yasanayake, C. N., & Denevi, B. W. (2020). Lunar
1061 Agglutinate Glass Composition and Implications for Agglutinate Formation (Abstract P054-
1062 0016). Presented at the AGU Fall Meeting 2020. Retrieved from
1063 https://agu.confex.com/agu/fm20/meetingapp.cgi/Paper/765987
1064 Basu, A., McKay, D. S., Griffiths, S. A., & Nace, G. (1982). Regolith maturation on the earth
1065 and the moon with an example from Apollo 15. In *Lunar and Planetary Science Conference*
1066 *Proceedings* (Vol. 12, pp. 433–449).
1067 Basu, A., Wentworth, S. J., & McKay, D. S. (2002). Heterogeneous agglutinitic glass and the
1068 fusion of the finest fraction (F3) model. *Meteoritics & Planetary Science*, *37*(12), 1835–
1069 1842. https://doi.org/10.1111/j.1945-5100.2002.tb01167.x
1070 Britt, D. T., & Pieters, C. M. (1994). Darkening in black and gas-rich ordinary chondrites: The
1071 spectral effects of opaque morphology and distribution. *Geochimica et Cosmochimica Acta*,
1072 *58*(18), 3905–3919. https://doi.org/10.1016/0016-7037(94)90370-0
1073 Bruegge, C., Chrien, N., & Haner, D. (2001). A Spectralon BRF data base for MISR calibration
1074 applications. *Remote Sensing of Environment*, *77*(3), 354–366.
1075 https://doi.org/10.1016/S0034-4257(01)00214-0
1076 Burgess, K., & Stroud, R. (2017). Glassy with a Chance of Nanophase Iron: Space Weathering
1077 of Lunar Soil as Observed with Aberration-Corrected Scanning Transmission Electron
1078 Microscopy. Microscopy Today, 25(3), 32–39. https://doi.org/10.1017/S1551929517000372

1079 Burgess, K. D., & Stroud, R. M. (2018). Coordinated Nanoscale Compositional and Oxidation
1080 State Measurements of Lunar Space-Weathered Material. Journal of Geophysical Research:
1081 Planets, 123(8), 2022–2037. https://doi.org/10.1029/2018JE005537
1082 Carrier, W. D. (2003). Particle Size Distribution of Lunar Soil. *Journal of Geotechnical and*
1083 *Geoenvironmental Engineering*, *129*(10), 956–959. https://doi.org/10.1061/(ASCE)1090-
1084 0241(2003)129:10(956)
1085 Cassidy, W., & Hapke, B. (1975). Effects of darkening processes on surfaces of airless bodies.
1086 *Icarus*, *25*(3), 371–383. https://doi.org/10.1016/0019-1035(75)90002-0
1087 Christoffersen, R., McKay, D. S., & Keller, L. P. (1996). Microstructure, chemistry, and origin of
1088 grain rims on ilmenite from the lunar soil finest fraction. *Meteoritics & Planetary Science*,
1089 *31*(6), 835–848. https://doi.org/10.1111/j.1945-5100.1996.tb02117.x
1090 Clark, B. E., Lucey, P., Helfenstein, P., Bell Iii, J. F., Peterson, C., Veverka, J., et al. (2001).
1091 Space weathering on Eros: Constraints from albedo and spectral measurements of Psyche
1092 crater. *Meteoritics & Planetary Science*, *36*(12), 1617–1637. https://doi.org/10.1111/j.1945-
1093 5100.2001.tb01853.x
1094 Conel, J. E., & Nash, D. B. (1970). Spectral reflectance and albedo of Apollo 11 lunar samples:
1095 Effects of irradiation and vitrification and comparison with telescopic observations.
1096 *Geochimica et Cosmochimica Acta Supplement*, *1*, 2013.
1097 Denevi, B. W., Lucey, P. G., & Sherman, S. B. (2008). Radiative transfer modeling of near-
1098 infrared spectra of lunar mare soils: Theory and measurement. *Journal of Geophysical*
1099 *Research: Planets*, *113*(E2). https://doi.org/10.1029/2007JE002929

1100 Denevi, Brett W., Noble, S. K., Christoffersen, R., Thompson, M. S., Glotch, T. D., Blewett, D.
1101 T., et al. (2023). Space Weathering At The Moon. Reviews in Mineralogy and
1102 Geochemistry, 89(1), 611–650. https://doi.org/10.2138/rmg.2023.89.14
1103 Fischer, E. M. (1995). *Quantitative compositional analysis of the lunar surface from reflectance*
1104 *spectroscopy: Iron, aluminum, and model for removing the optical effects of space*
1105 *weathering* (Ph.D.). Brown University, United States -- Rhode Island. Retrieved from
1106 https://www.proquest.com/docview/304164546/abstract/BA6999E74DEA4539PQ/1
1107 Hapke, B. (1973). Darkening of silicate rock powders by solar wind sputtering. *The Moon*, *7*(3),
1108 342–355. https://doi.org/10.1007/BF00564639
1109 Hapke, B. (2001). Space weathering from Mercury to the asteroid belt. *Journal of Geophysical*
1110 *Research: Planets*, *106*(E5), 10039–10073. https://doi.org/10.1029/2000JE001338
1111 Hapke, B., Cassidy, W., & Wells, E. (1975). Effects of vapor-phase deposition processes on the
1112 optical, chemical, and magnetic properties OE the lunar regolith. *The Moon*, *13*(1), 339–
1113 353. https://doi.org/10.1007/BF00567525
1114 Harris, C. R., Millman, K. J., van der Walt, S. J., Gommers, R., Virtanen, P., Cournapeau, D., et
1115 al. (2020). Array programming with NumPy. Nature, 585(7825), 357–362.
1116 https://doi.org/10.1038/s41586-020-2649-2
1117 Heiken, G., & McKay, D. S. (1974). Petrography of Apollo 17 soils. In *In: Lunar Science*
1118 *Conference, 5th, Houston, Tex., March 18-22, 1974, Proceedings. Volume 1.(A75-39540*
1119 *19-91) New York, Pergamon Press, Inc., 1974, p. 843-860.* (Vol. 5, pp. 843–860).
1120 Housley, R. M., Grant, R. W., & Abdel-Gawad, M. (1972). Study of excess Fe metal in the lunar
1121 fines by magnetic separation Mössbauer spectroscopy, and microscopic examination. In
1122 *Lunar and Planetary Science Conference Proceedings* (Vol. 3, p. 392).

1123 Housley, R. M., Cirlin, E. H., Paton, N. E., & Goldberg, I. B. (1974). Solar wind and
1124 micrometeorite alteration of the lunar regolith. In *Lunar and planetary science conference*
1125 *proceedings* (Vol. 5, pp. 2623–2642).
1126 Housley, R. M., Cirlin, E. H., Goldberg, I. B., Crowe, H., Weeks, R. A., & Perhac, R. (1975).
1127 Ferromagnetic resonance as a method of studying the micrometeorite bombardment history
1128 of the lunar surface. In *Lunar and Planetary Science Conference Proceedings* (Vol. 6, pp.
1129 3173–3186).
1130 Housley, R. M., Cirlin, E. H., Goldberg, I. B., & Crowe, H. (1976). Ferromagnetic resonance
1131 studies of lunar core stratigraphy. In *Lunar and Planetary Science Conference Proceedings*
1132 (Vol. 7, pp. 13–26).
1133 Housley, R. M., Grant, R. W., & Paton, N. E. (1973). Origin and characteristics of excess Fe
1134 metal in lunar glass welded aggregates. In *Proceedings of the Lunar Science Conference,*
1135 *vol. 4, p. 2737* (Vol. 4, p. 2737).
1136 Hunter, J. D. (2007). Matplotlib: A 2D Graphics Environment. Computing in Science &
1137 Engineering, 9(3), 90–95. https://doi.org/10.1109/MCSE.2007.55
1138 James, C. L., Letsinger, S. L., Basu, A., Wentworth, S. J., & McKay, D. S. (2002). Size
1139 Distribution of Fe0 Globules in Lunar Agglutinitic Glass, 1827. Presented at the Lunar and
1140 Planetary Science Conference.
1141 Keller, L. P., & Clemett, S. J. (2001). Formation of Nanophase Iron in the Lunar Regolith, 2097.
1142 Presented at the Lunar and Planetary Science Conference.
1143 Keller, L. P., Wentworth, S. J., & McKay, D. S. (1998). Space Weathering: Reflectance
1144 Spectroscopy and TEM Analysis of Individual Lunar Soil Grains. In *Lunar and Planetary*
1145 *Science Conference* (p. 1762).

1146 Keller, Lindsay P., & McKay, D. S. (1993). Discovery of Vapor Deposits in the Lunar Regolith.
1147 *Science*, *261*(5126), 1305–1307. https://doi.org/10.1126/science.261.5126.1305
1148 Keller, Lindsay P., & McKay, D. S. (1997). The nature and origin of rims on lunar soil grains.
1149 *Geochimica et Cosmochimica Acta*, *61*(11), 2331–2341. https://doi.org/10.1016/S0016-
1150 7037(97)00085-9
1151 Keller, Lindsay P., Berger, E. L., Zhang, S., & Christoffersen, R. (2021). Solar energetic particle
1152 tracks in lunar samples: A transmission electron microscope calibration and implications for
1153 lunar space weathering. *Meteoritics & Planetary Science*, *56*(9), 1685–1707.
1154 https://doi.org/10.1111/maps.13732
1155 Labotka, T. C., Kempa, M. J., White, C., Papike, J. J., & Laul, J. C. (1980). The lunar regolith-
1156 Comparative petrology of the Apollo sites. In *Lunar and Planetary Science Conference*
1157 *Proceedings* (Vol. 11, pp. 1285–1305).
1158 Lawrence, S. J., & Lucey, P. G. (2007). Radiative transfer mixing models of meteoritic
1159 assemblages. *Journal of Geophysical Research: Planets*, *112*(E7).
1160 https://doi.org/10.1029/2006JE002765
1161 Li, S., & Li, L. (2011). Radiative transfer modeling for quantifying lunar surface minerals,
1162 particle size, and submicroscopic metallic Fe. *Journal of Geophysical Research: Planets*,
1163 *116*(E9). https://doi.org/10.1029/2011JE003837
1164 Lucey, P., Korotev, R. L., Gillis, J. J., Taylor, L. A., Lawrence, D., Campbell, B. A., et al.
1165 (2006). Understanding the Lunar Surface and Space-Moon Interactions. *Reviews in*
1166 *Mineralogy and Geochemistry*, *60*(1), 83–219. https://doi.org/10.2138/rmg.2006.60.2

1167 Lucey, P. G., & Riner, M. A. (2011). The optical effects of small iron particles that darken but do
1168 not redden: Evidence of intense space weathering on Mercury. *Icarus*, *212*(2), 451–462.
1169 https://doi.org/10.1016/j.icarus.2011.01.022
1170 McKay, D. S., Heiken, G. H., Taylor, R. M., Clanton, U. S., Morrison, D. A., & Ladle, G. H.
1171 (1972). Apollo 14 soils: Size distribution and particle types. In *Lunar and Planetary Science*
1172 *Conference Proceedings* (Vol. 3, p. 983).
1173 McKay, D. S., Heiken, G., Basu, A., Blanford, G., Simon, S., Reedy, R., et al. (1991). The lunar
1174 regolith. *Lunar Sourcebook*, *567*, 285–356.
1175 Meyer, C. (2005). Lunar Sample Compendium. *NASA STI/Recon Technical Report N*, *6*.
1176 Retrieved from https://curator.jsc.nasa.gov/lunar/lsc/
1177 Milliken, R. E., Hiroi, T., & Patterson, W. (2016). The NASA reflectance experiment laboratory
1178 (RELAB) facility: Past, present, and future. In *47th Annual Lunar and Planetary Science*
1179 *Conference* (p. 2058).
1180 Morris, R. V. (1976). Surface exposure indices of lunar soils-A comparative FMR study. In
1181 *Lunar and Planetary Science Conference Proceedings* (Vol. 7, pp. 315–335).
1182 Morris, R. V. (1977). Origin and evolution of the grain-size dependence of the concentration of
1183 fine-grained metal in lunar soils-The maturation of lunar soils to a steady-state stage. In
1184 *Lunar and Planetary Science Conference Proceedings* (Vol. 8, pp. 3719–3747).
1185 Morris, R. V. (1978). The surface exposure (maturity) of lunar soils-Some concepts and Is/FeO
1186 compilation. In *Lunar and Planetary Science Conference Proceedings* (Vol. 9, pp. 2287–
1187 2297).
1188 Morris, R. V. (1980). Origins and size distribution of metallic iron particles in the lunar regolith.
1189 In *In: Lunar and Planetary Science Conference, 11th, Houston, TX, March 17-21, 1980,*

Proceedings. Volume 2.(A82-22296 09-91) New York, Pergamon Press, 1980, p. 1697-1712. (Vol. 11, pp. 1697–1712).

Mustard, J. F., Pieters, C. M., Isaacson, P. J., Head, J. W., Besse, S., Clark, R. N., et al. (2011). Compositional diversity and geologic insights of the Aristarchus crater from Moon Mineralogy Mapper data. *Journal of Geophysical Research: Planets*, *116*(E6). https://doi.org/10.1029/2010JE003726

Nash, D. B., & Conel, J. E. (1973). Vitrification darkening of rock powders: implications for optical properties of the lunar surface. *Moon*, *8*, 346–364. https://doi.org/10.1007/BF00581729

Nettles, J. W., Staid, M., Besse, S., Boardman, J., Clark, R. N., Dhingra, D., et al. (2011). Optical maturity variation in lunar spectra as measured by Moon Mineralogy Mapper data. *Journal of Geophysical Research: Planets*, *116*(E9). https://doi.org/10.1029/2010JE003748

Nimura, T., Hiroi, T., & Pieters, C. M. (2008). An improved scheme for modeling the reflectance spectra of space-weathered regoliths. *Earth, Planets and Space*, *60*(4), 271–275. https://doi.org/10.1186/BF03352791

Noble, S. K., Pieters, C. M., Taylor, L. A., Morris, R. V., Allen, C. C., McKAY, D. S., & Keller, L. P. (2001). The optical properties of the finest fraction of lunar soil: Implications for space weathering. *Meteoritics & Planetary Science*, *36*(1), 31–42. https://doi.org/10.1111/j.1945-5100.2001.tb01808.x

Noble, S. K., Pieters, C. M., & Keller, L. P. (2007). An experimental approach to understanding the optical effects of space weathering. *Icarus*, *192*(2), 629–642. https://doi.org/10.1016/j.icarus.2007.07.021

1212 Pieters, C. M., Fischer, E. M., Rode, O., & Basu, A. (1993). Optical effects of space weathering:
1213 The role of the finest fraction. *Journal of Geophysical Research: Planets*, *98*(E11), 20817–
1214 20824. https://doi.org/10.1029/93JE02467
1215 Pieters, Carle M., & Noble, S. K. (2016). Space weathering on airless bodies. *Journal of*
1216 *Geophysical Research: Planets*, *121*(10), 1865–1884.
1217 https://doi.org/10.1002/2016JE005128
1218 Pieters, Carlé M., Stankevich, D. G., Shkuratov, Yu. G., & Taylor, L. A. (2002). Statistical
1219 Analysis of the Links among Lunar Mare Soil Mineralogy, Chemistry, and Reflectance
1220 Spectra. *Icarus*, *155*(2), 285–298. https://doi.org/10.1006/icar.2001.6749
1221 Poulet, F., & Erard, S. (2004). Nonlinear spectral mixing: Quantitative analysis of laboratory
1222 mineral mixtures. *Journal of Geophysical Research: Planets*, *109*(E2).
1223 https://doi.org/10.1029/2003JE002179
1224 Poulet, F., Cuzzi, J. N., Cruikshank, D. P., Roush, T., & Dalle Ore, C. M. (2002). Comparison
1225 between the Shkuratov and Hapke Scattering Theories for Solid Planetary Surfaces:
1226 Application to the Surface Composition of Two Centaurs. *Icarus*, *160*(2), 313–324.
1227 https://doi.org/10.1006/icar.2002.6970
1228 Python Software Foundation. (2022, December 6). Python 3.9.16 documentation (Version
1229 3.9.16). Retrieved from https://docs.python.org/release/3.9.16/
1230 Shkuratov, Y., Starukhina, L., Hoffmann, H., & Arnold, G. (1999). A Model of Spectral Albedo
1231 of Particulate Surfaces: Implications for Optical Properties of the Moon. *Icarus*, *137*(2),
1232 235–246. https://doi.org/10.1006/icar.1998.6035
1233 Simon, S. B., & Papike, J. J. (1981). The Lunar regolith: comparative petrology of the Apollo
1234 and Luna soils. In *Lunar and Planetary Science Conference* (Vol. 12, pp. 984–986).

1235 Simon, Steven B., Papike, J. J., & Laul, J. C. (1981). The lunar regolith-Comparative studies of
1236 the Apollo and Luna sites. Petrology of soils from Apollo 17, Luna 16, 20, and 24. In *Lunar*
1237 *and Planetary Science Conference Proceedings* (Vol. 12, pp. 371–388).
1238 Taylor, L. A., & Cirlin, E. H. (1985). A review of ESR studies on lunar samples. In M. Ikeya &
1239 T. Miki (Eds.), *ESR Dating and Dosimetry* (pp. 19–29). Tokyo: IONICS.
1240 Taylor, L. A., Patchen, A., Taylor, D.-H. S., Chambers, J. G., & McKay, D. S. (1996). X-Ray
1241 Digital Imaging Petrography of Lunar Mare Soils: Modal Analyses of Minerals and Glasses.
1242 *Icarus*, *124*(2), 500–512. https://doi.org/10.1006/icar.1996.0226
1243 Taylor, L. A., Pieters, C. M., Keller, L. P., Morris, R. V., & McKay, D. S. (2001a). Lunar Mare
1244 Soils: Space weathering and the major effects of surface-correlated nanophase Fe. *Journal*
1245 *of Geophysical Research: Planets*, *106*(E11), 27985–27999.
1246 https://doi.org/10.1029/2000JE001402
1247 Taylor, L. A., Pieters, C., Keller, L. P., Morris, R. V., McKAY, D. S., Patchen, A., & Wentworth,
1248 S. (2001b). The effects of space weathering on Apollo 17 mare soils: Petrographie and
1249 chemical characterization. *Meteoritics & Planetary Science*, *36*(2), 285–299.
1250 https://doi.org/10.1111/j.1945-5100.2001.tb01871.x
1251 Taylor, L. A., Pieters, C., Patchen, A., Taylor, D.-H. S., Morris, R. V., Keller, L. P., & McKay,
1252 D. S. (2010). Mineralogical and chemical characterization of lunar highland soils: Insights
1253 into the space weathering of soils on airless bodies. *Journal of Geophysical Research:*
1254 *Planets*, *115*(E2). https://doi.org/10.1029/2009JE003427
1255 The pandas development team. (2023, January 19). pandas-dev/pandas: Pandas (Version v1.5.3).
1256 Zenodo. https://doi.org/10.5281/zenodo.7549438

1257 Thompson, M. S., Zega, T. J., Becerra, P., Keane, J. T., & Byrne, S. (2016). The oxidation state
1258 of nanophase Fe particles in lunar soil: Implications for space weathering. Meteoritics &
1259 Planetary Science, 51(6), 1082–1095. https://doi.org/10.1111/maps.12646
1260 Thompson, M. S., Zega, T. J., & Howe, J. Y. (2017). In situ experimental formation and growth
1261 of Fe nanoparticles and vesicles in lunar soil. *Meteoritics & Planetary Science*, *52*(3), 413–
1262 427. https://doi.org/10.1111/maps.12798
1263 Vaniman, D. T., & Papike, J. J. (1977). The Apollo 17 drill core-Modal petrology and glass
1264 chemistry/sections 70007, 70008, 70009. In *In: Lunar Science Conference, 8th, Houston,*
1265 *Tex., March 14-18, 1977, Proceedings. Volume 3.(A78-41551 18-91) New York, Pergamon*
1266 *Press, Inc., 1977, p. 3161-3193.* (Vol. 8, pp. 3161–3193).
1267 Via, W. N., & Taylor, L. A. (1976a). Agglutinate Formation: Is Chemical Fractionation
1268 Involved? In *Lunar and Planetary Science Conference* (Vol. 7).
1269 Via, W. N., & Taylor, L. A. (1976b). Chemical aspects of agglutinate formation-Relationships
1270 between agglutinate composition and the composition of the bulk soil. In *Lunar and*
1271 *Planetary Science Conference Proceedings* (Vol. 7, pp. 393–403).
1272 Warell, J., & Davidsson, B. J. R. (2010). A Hapke model implementation for compositional
1273 analysis of VNIR spectra of Mercury. *Icarus*, *209*(1), 164–178.
1274 https://doi.org/10.1016/j.icarus.2009.11.037
1275 Wells, E., & Hapke, B. (1977). Lunar Soil: Iron and Titanium Bands in the Glass Fraction.
1276 *Science*, *195*(4282), 977–979. https://doi.org/10.1126/science.195.4282.977
1277 Yang, Y., Li, S., Milliken, R. E., Zhang, H., Robertson, K., & Hiroi, T. (2019). Phase Functions
1278 of Typical Lunar Surface Minerals Derived for the Hapke Model and Implications for

Visible to Near-Infrared Spectral Unmixing. *Journal of Geophysical Research: Planets*, *124*(1), 31–60. https://doi.org/10.1029/2018JE005713

Zhang, H., Yang, Y., Jin, W., Liu, C., & Hsu, W. (2014). Effects of Spectralon absorption on reflectance spectra of typical planetary surface analog materials. *Optics Express*, *22*(18), 21280–21291. https://doi.org/10.1364/OE.22.021280

Figure Captions

Figure 1. Scanning electron microscope images of agglutinates from the 125–250 μm size fraction (contrast stretched for clarity). **Top row:** whole grains from two soils (**(A)** 67461, **(B)** 79221) illustrate their three-dimensional structure as misshapen agglomerates of glass, mineral, and lithic fragments**. Bottom row:** polished carbon-coated grain mounts from two soils (**(C)** 67461, **(D)** 79221) highlight the vesicular internal structure.

Figure 2. Microscope images of **(A)** magnetically separated 125–250 μm agglutinates from sample 62231 and **(B)** the corresponding non-agglutinates. The images have been color corrected to approximate appearance under white light.

Figure 3. Soil separates produced by the magnetic separator (soil 62231, 75–125 μm size fraction), imaged **(top row)** on weighing paper and **(bottom row)** under a binocular microscope. **(A, D)** The least magnetic particles, which fell down the chute and into the bin further from the magnet, are visually bright and contain largely mineral fragments and no agglutinates; **(B, E)** the moderately magnetic particles, which fell down the chute and into the bin closer to the magnet, are intermediate in brightness and contain mineral and breccia fragments with few agglutinates; and **(C, F)** the highly magnetic particles, which were suspended in the chute by the magnet, are visually darkest and are rich in agglutinates.

Figure 4. Estimated agglutinate abundance vs. soil maturity for the lunar soils. All agglutinates were magnetic–manual separated except for the manually separated 62231.52 (denoted by a triangle marker, and likely overestimated due to substantial contamination of the agglutinate separate with non-agglutinate particles). Note that, while the agglutinate abundance values measured in this study are for the 125–250 μm size fraction, the soil maturity values from Morris (1978) are for the <250 μm size fraction.

Figure 5. Microscope images of the 125–250 μm agglutinate separates from soil 62231, yielded by **(A)** the magnetic–manual method and **(B)** the manual sorting method, showing the former's higher purity (fewer non-agglutinate particles). The images have been color corrected to approximate appearance under white light. Particles we categorize as non-agglutinates are circled in blue. Note that categorizing particles as either agglutinates or non-agglutinates is an oversimplification, albeit a necessary one. For example, the circled "non-agglutinate" particle in (A) is categorized as such due to its predominantly smooth texture, but it does have a small amount of rough-textured agglutinitic material fused onto its upper side.

Figure 6. Microscopic images of 125–250 μm non-agglutinate separates from four mature soils of different composition: **(A)** 62231 (highlands), **(B)** 14259 (non-mare), **(C)** 15041 (low-Ti mare), and **(D)** 79221 (high-Ti mare). Here and in Figures 7 and 8, each image was collected with the same illumination conditions and is shown with the same relative contrast stretch. The images have been color corrected to approximate appearance under white light.

Figure 7. Microscopic images of 125–250 μm agglutinate separates from four mature soils of different composition: **(A)** 62231 (highlands), **(B)** 14259 (non-mare), **(C)** 15041 (low-Ti mare), and **(D)** 79221 (high-Ti mare). Here and in Figures 6 and 8, each image was collected with the

same illumination conditions and is shown with the same relative contrast stretch. The images have been color corrected to approximate appearance under white light.

Figure 8. Microscope images of 125–250 μm agglutinate separates (left) and non-agglutinates (right) from Apollo 16 soils of different maturities: **(A, B)** immature soil 67461 (I_S/FeO = 25), **(C, D)** submature soil 61141 (I_S/FeO = 56), and **(E, F)** mature soil 62231 (I_S/FeO = 91). Here and in Figures 6 and 7, each image was collected with the same illumination conditions and is shown with the same relative contrast stretch. The images have been color corrected to approximate appearance under white light.

Figure 9. Reflectance spectra of the 125–250 μm unsorted, non-agglutinate, and agglutinate separates for the six soils. Each separate's mean spectrum (thick dark line) is the average of multiple individual measurements (thin faint lines). The number of measurements contributing to each mean is indicated in parentheses.

Figure 10. Same as Figure 9, but showing the mean reflectance spectra normalized to their values at 0.7 μm. The number of measurements contributing to each mean is indicated in parentheses, but these individual measurement spectra are not shown.

Figure 11. (top) Continuum ratio vs integrated 1 μm band depth and **(bottom)** albedo vs integrated 1 μm band depth for the mean reflectance spectra of the 125–250 μm unsorted, non-agglutinate, and agglutinate separates. Continuum ratio is defined as the ratio of 1550 nm reflectance to 750 nm reflectance, while albedo is measured by 1550 nm reflectance. Soil names are indicated by the annotations: 16i (67461, immature), 16s (61141, submature), 16m (62231, mature), 14 (14259), 15 (15041), 17 (79221). Dotted gray lines connect each soil's three separates: agglutinates, unsorted, non-agglutinates.

Figure 12. Reflectance spectra of the 125–250 μm unsorted, non-agglutinate, and agglutinate separates from the three Apollo 16 (highland) soils: immature soil 67461 (I_S/FeO = 25), submature soil 61141 (I_S/FeO = 56), and mature soil 62231 (I_S/FeO = 91). **(left)** Mean spectra and **(right)** the same spectra normalized to their values at 0.7 μm. The number of measurements contributing to each mean is indicated in parentheses, but these individual measurement spectra are not shown.

Figure 13. Reflectance spectra for two size fractions (125–250 μm and 75–125 μm) of unsorted, non-agglutinate, and agglutinate separates from the 62231 soil. **(left)** Mean spectra and **(right)** the same spectra normalized to their values at 0.7 μm. The number of measurements contributing to each mean is indicated in parentheses, but these individual measurement spectra are not shown.

Figure 14. Agglutinate abundance of soils in this study, as measured using different methods and for different size fractions. Data points are plotted at the average value of the measured size fraction, while the errors bars show the range of the size fraction. Note that ranges shown to extend down to 1 μm indicate finest fractions (e.g., <10 μm, not 1–10 μm). Data source abbreviations are as follows: LSCC = Lunar Soil Characterization Consortium (Taylor et al.,

2001a, 2010); B82 = Basu et al., 1982; T96 = Taylor et al., 1996; M72 = McKay et al., 1972; HM74 = Heiken and McKay, 1974; SP81 = Simon and Papike, 1981.

Figure 15. Comparison of reflectance spectra for 125–250 μm agglutinates (solid colored lines; this study) and npFe in silica gel (dashed/dotted black lines; Noble et al., 2007). Spectra are normalized to their reflectance values at 0.55 μm. Each of the four panels shows the same agglutinate spectra, but plotted alongside spectra of npFe with differing average size (8, 15, 35, 40 nm). Annotations next to each npFe spectrum denote npFe abundance (as a weight percentage).

Figure 1.

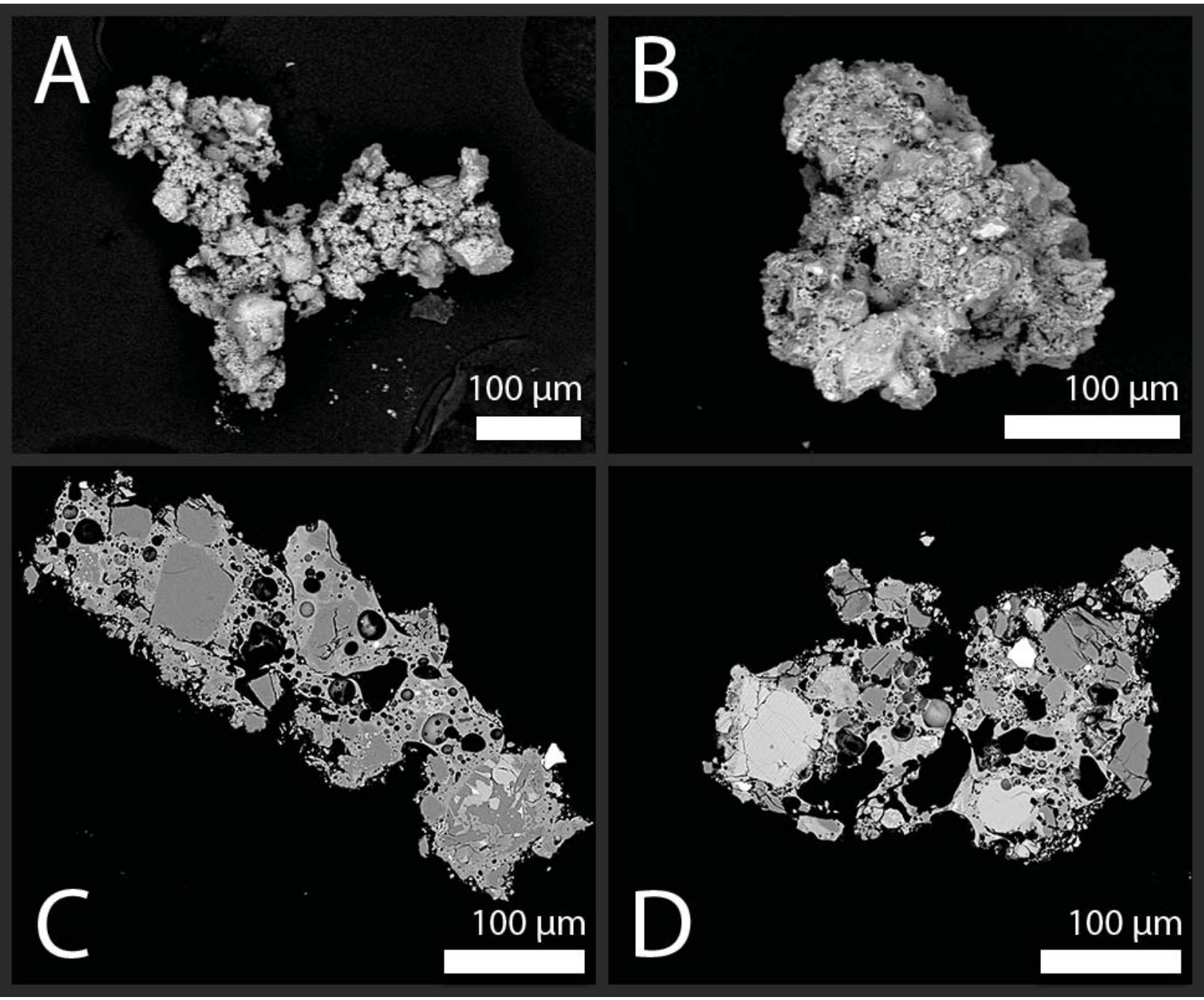
A
100 µm
B
100 µm
C
100 µm
D
100 µm

Figure 2.

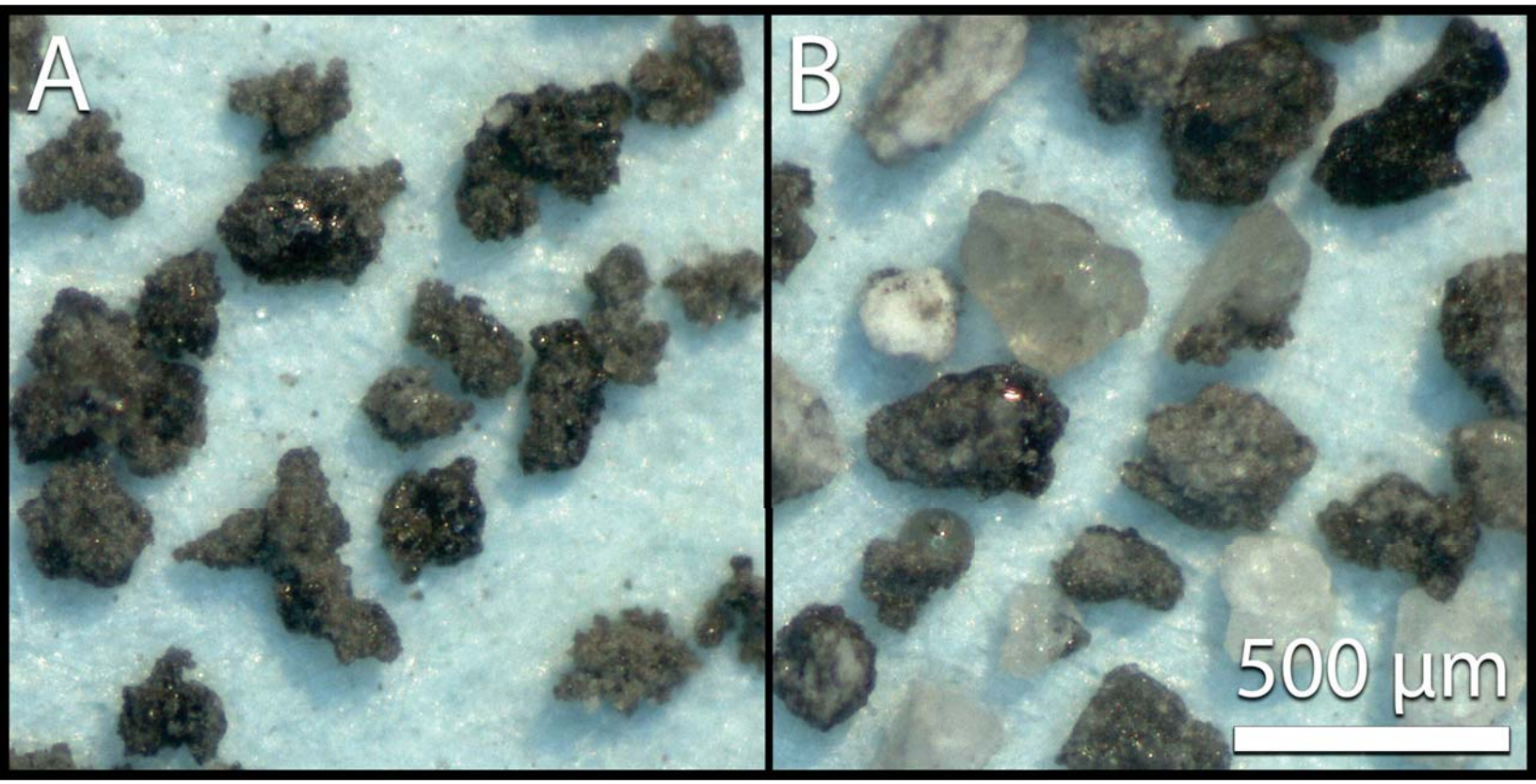
A
B
500 µm

Figure 3.

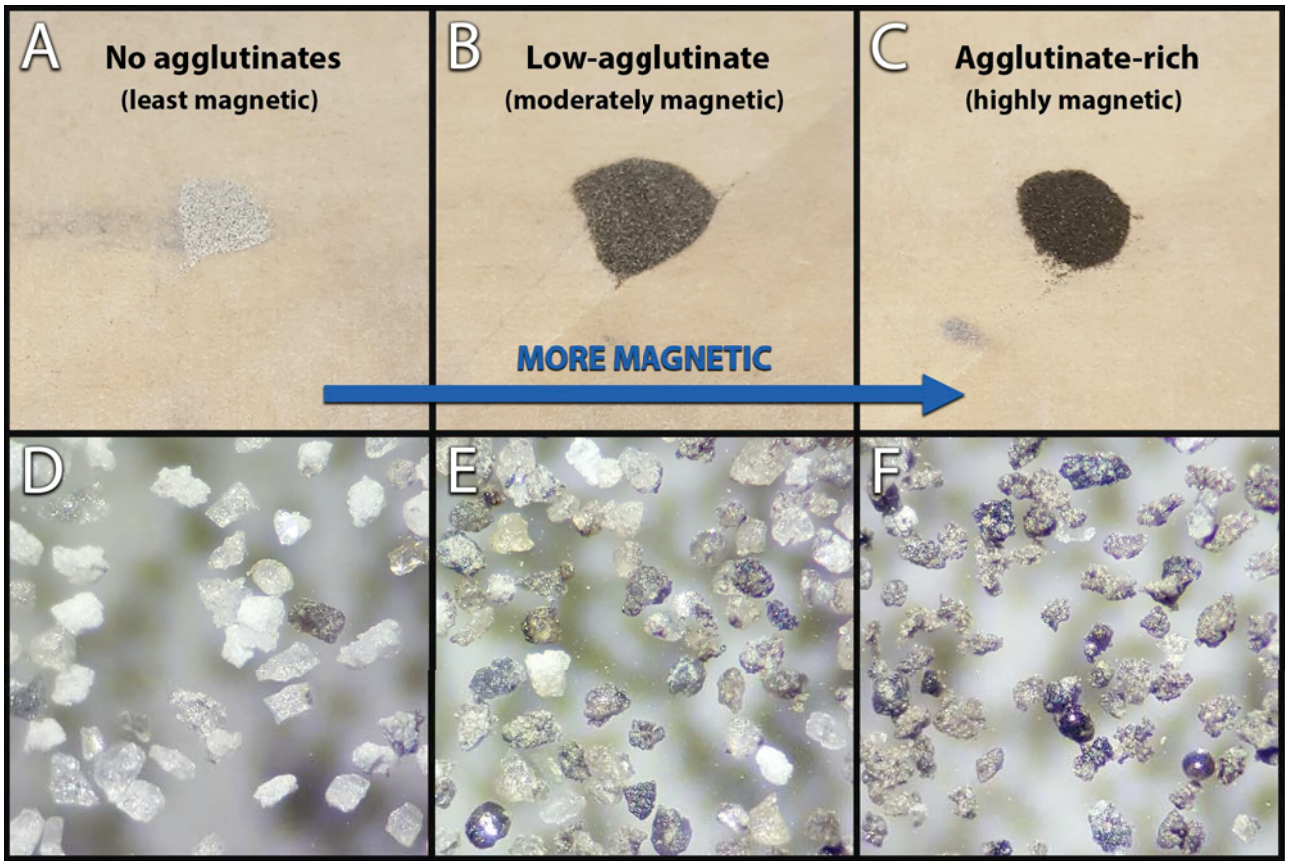
A
No agglutinates
(least magnetic)
B
Low-agglutinate
(moderately magnetic)
C
Agglutinate-rich
(highly magnetic)
MORE MAGNETIC
D
E
F

Figure 5.

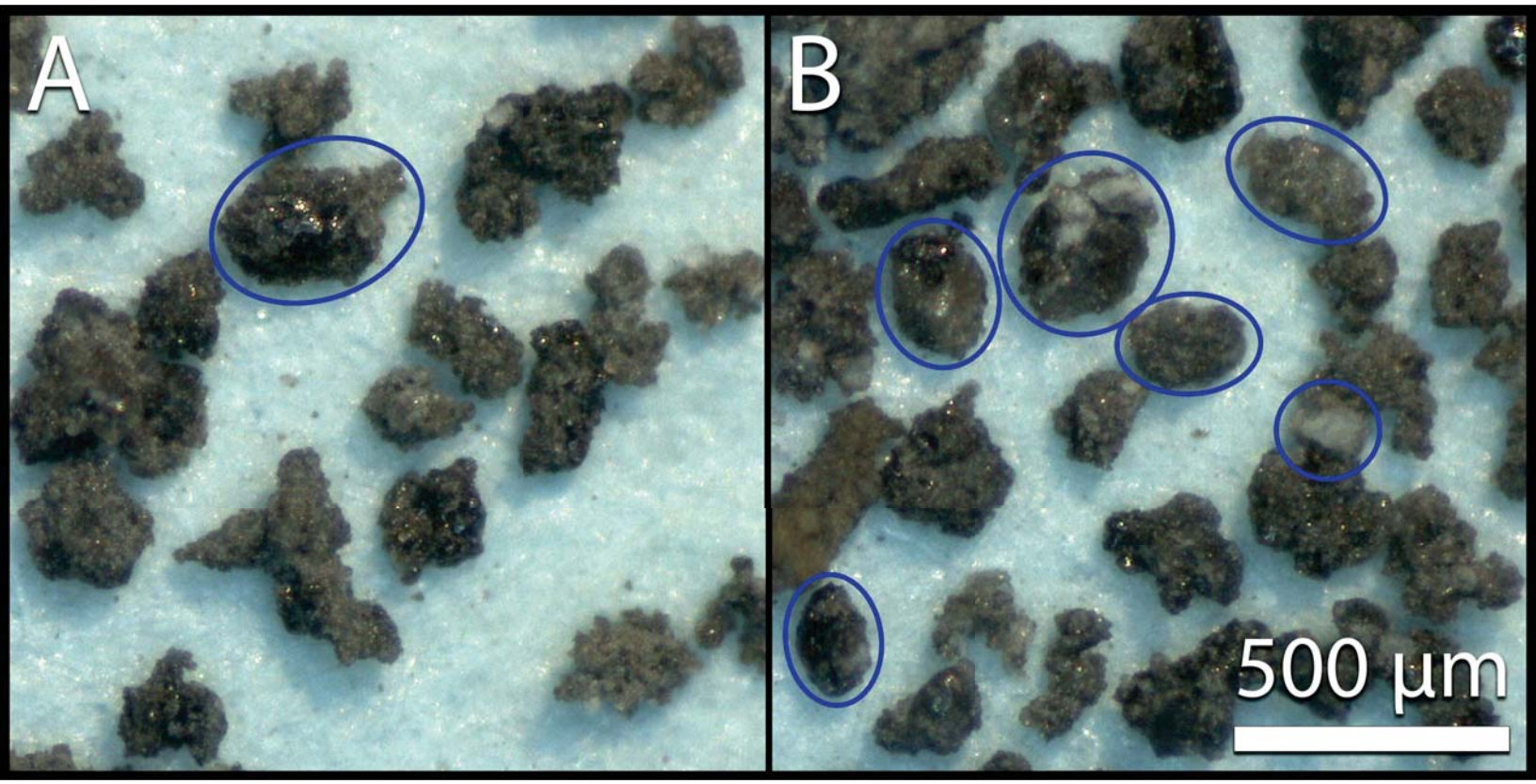
A
B
500 µm

Figure 6.

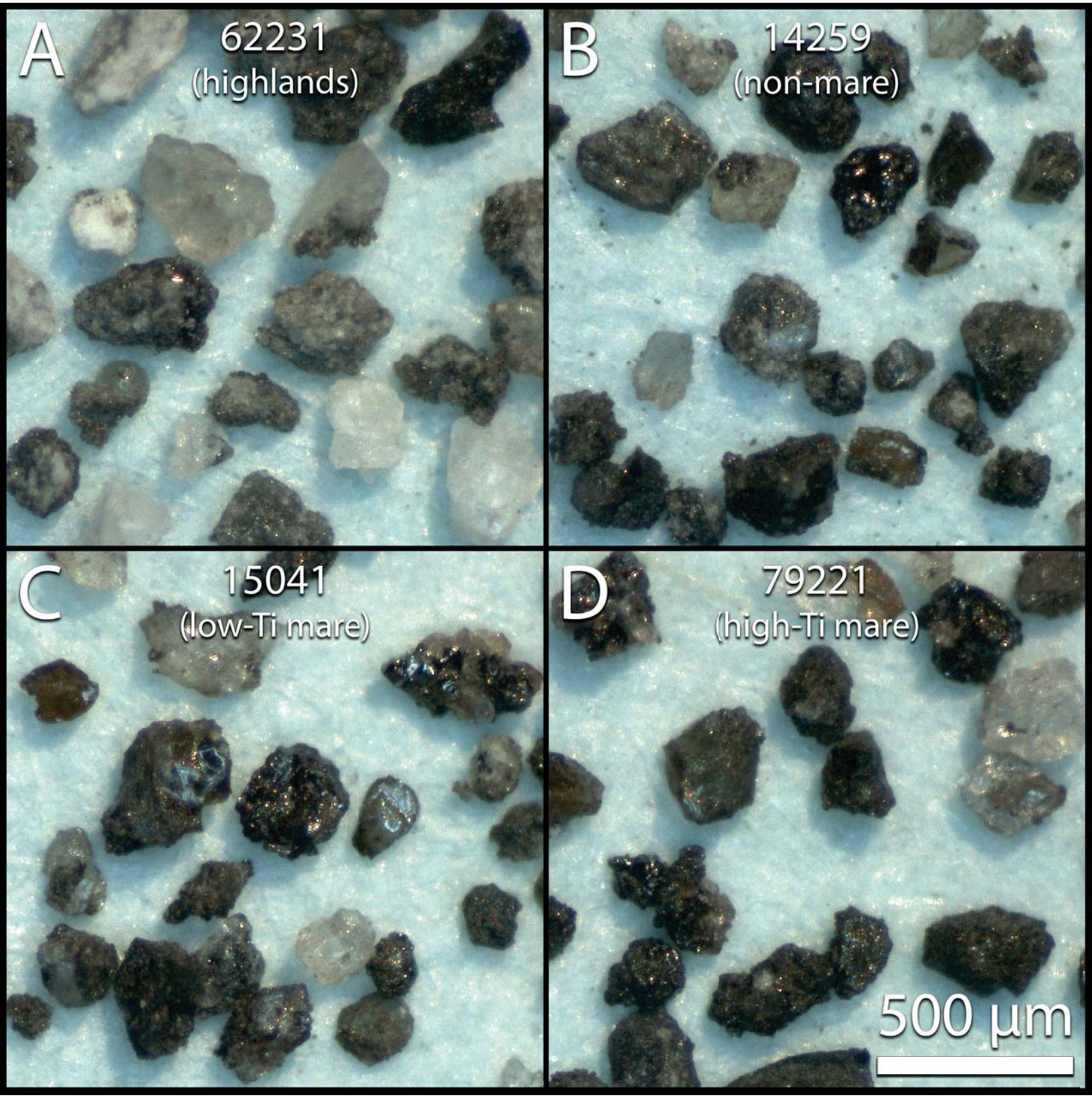
A
62231
(highlands)
B
14259
(non-mare)
C
15041
(low-Ti mare)
D
79221
(high-Ti mare)
500 µm

Figure 7.

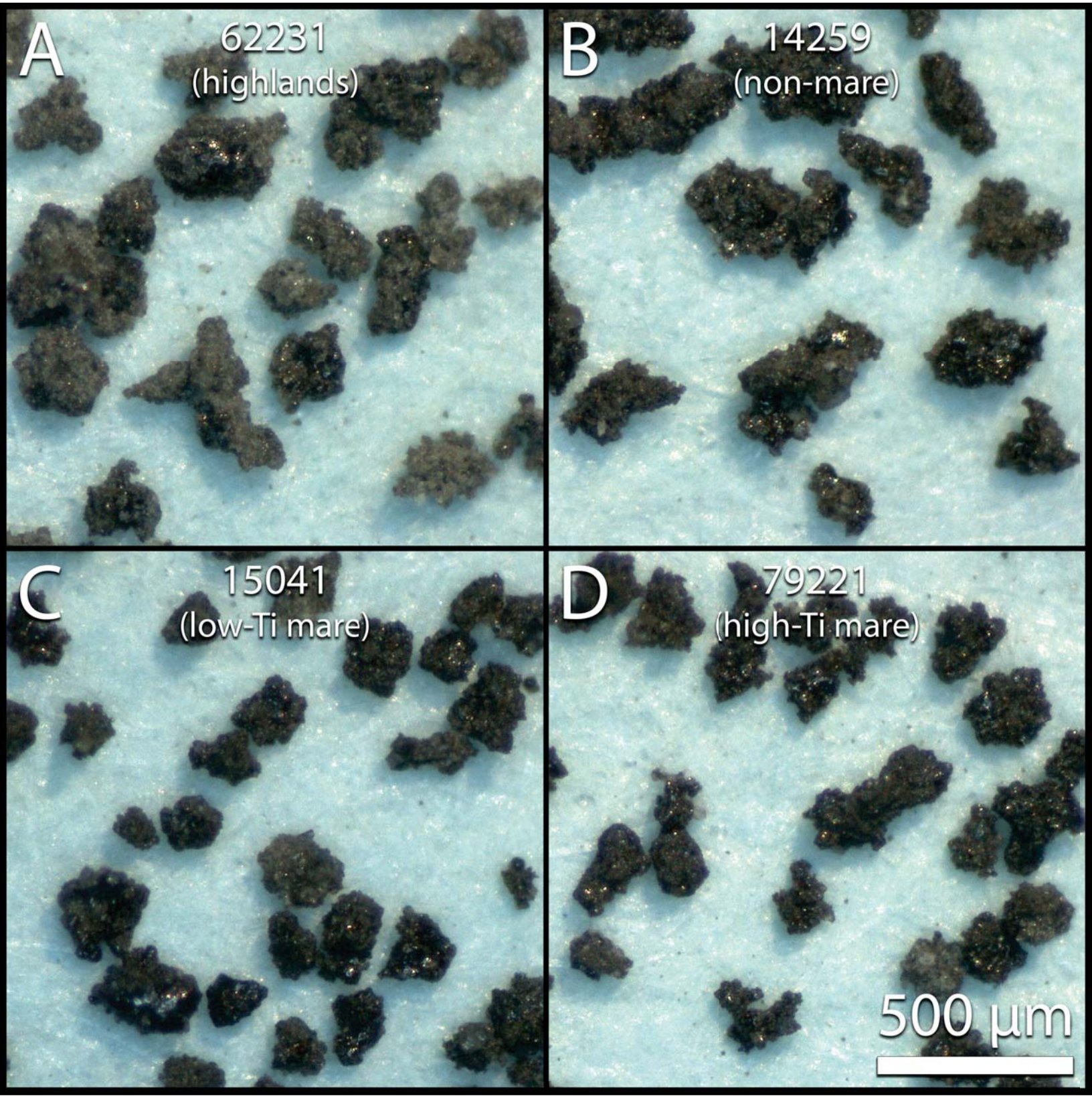
A
62231
(highlands)
B
14259
(non-mare)
C
15041
(low-Ti mare)
D
79221
(high-Ti mare)
500 µm

Figure 8.

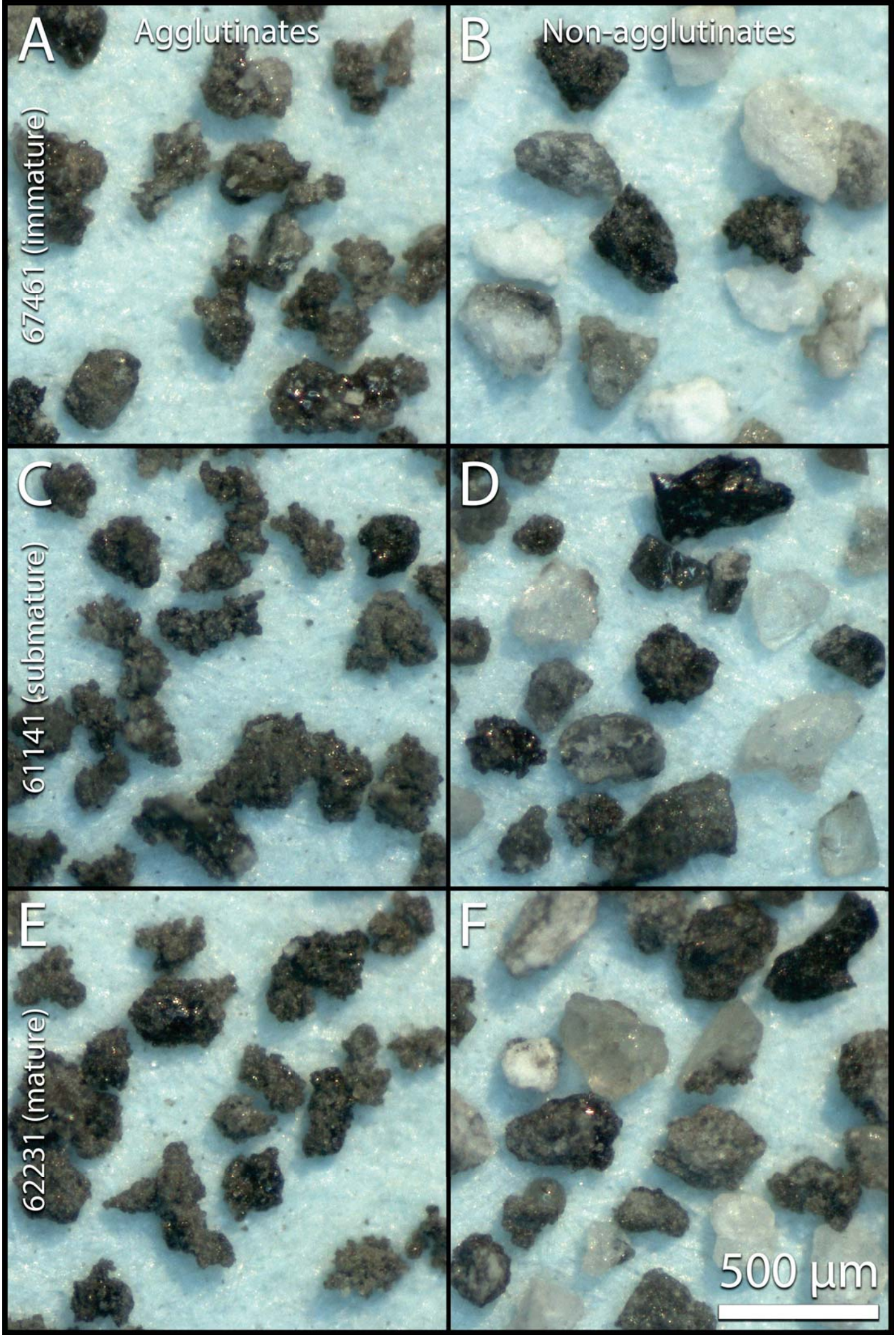
A
Agglutinates
67461 (immature)
B
Non-agglutinates
C
61141 (submature)
D
E
62231 (mature)
F
500 µm

Figure 4.

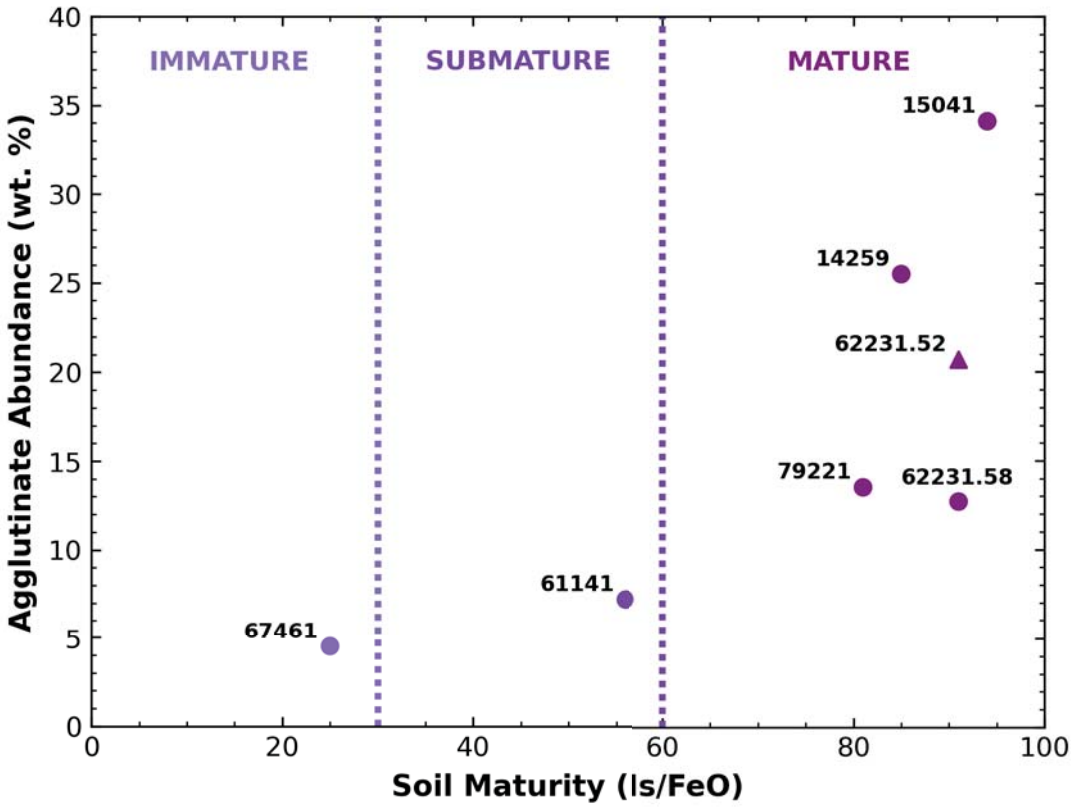
IMMATURE
SUBMATURE
MATURE
15041
14259
62231.52
79221
62231.58
61141
67461
Agglutinate Abundance (wt. %)
Soil Maturity (Is/FeO)
0
5
10
15
20
25
30
35
40
0
20
40
60
80
100

Figure 9.

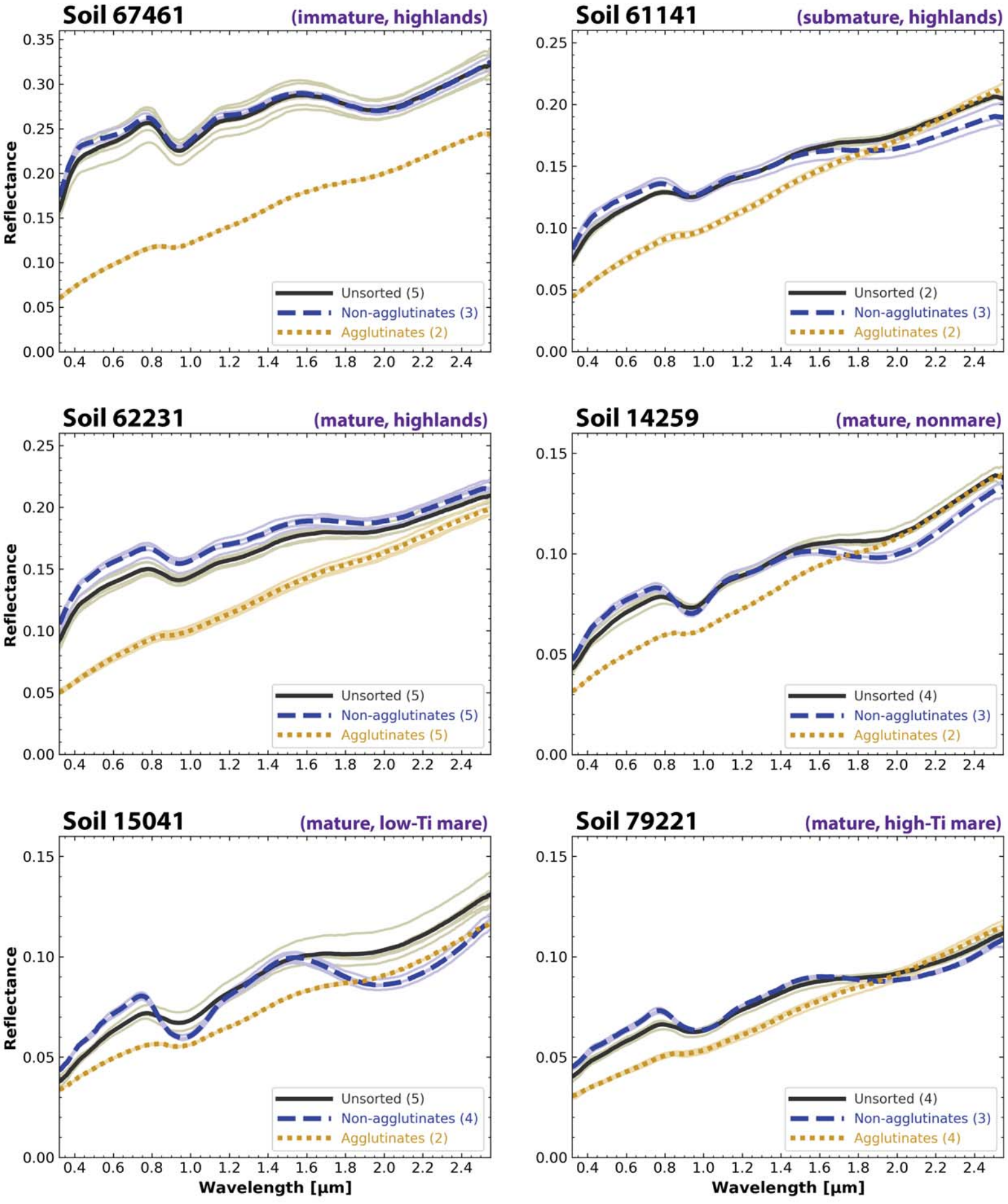
Soil 67461
(immature, highlands)
Unsorted (5)
Non-agglutinates (3)
Agglutinates (2)
Soil 61141
(submature, highlands)
Unsorted (2)
Non-agglutinates (3)
Agglutinates (2)
Soil 62231
(mature, highlands)
Unsorted (5)
Non-agglutinates (5)
Agglutinates (5)
Soil 14259
(mature, nonmare)
Unsorted (4)
Non-agglutinates (3)
Agglutinates (2)
Soil 15041
(mature, low-Ti mare)
Unsorted (5)
Non-agglutinates (4)
Agglutinates (2)
Soil 79221
(mature, high-Ti mare)
Unsorted (4)
Non-agglutinates (3)
Agglutinates (4)
Reflectance
Wavelength [μm]

Figure 10.

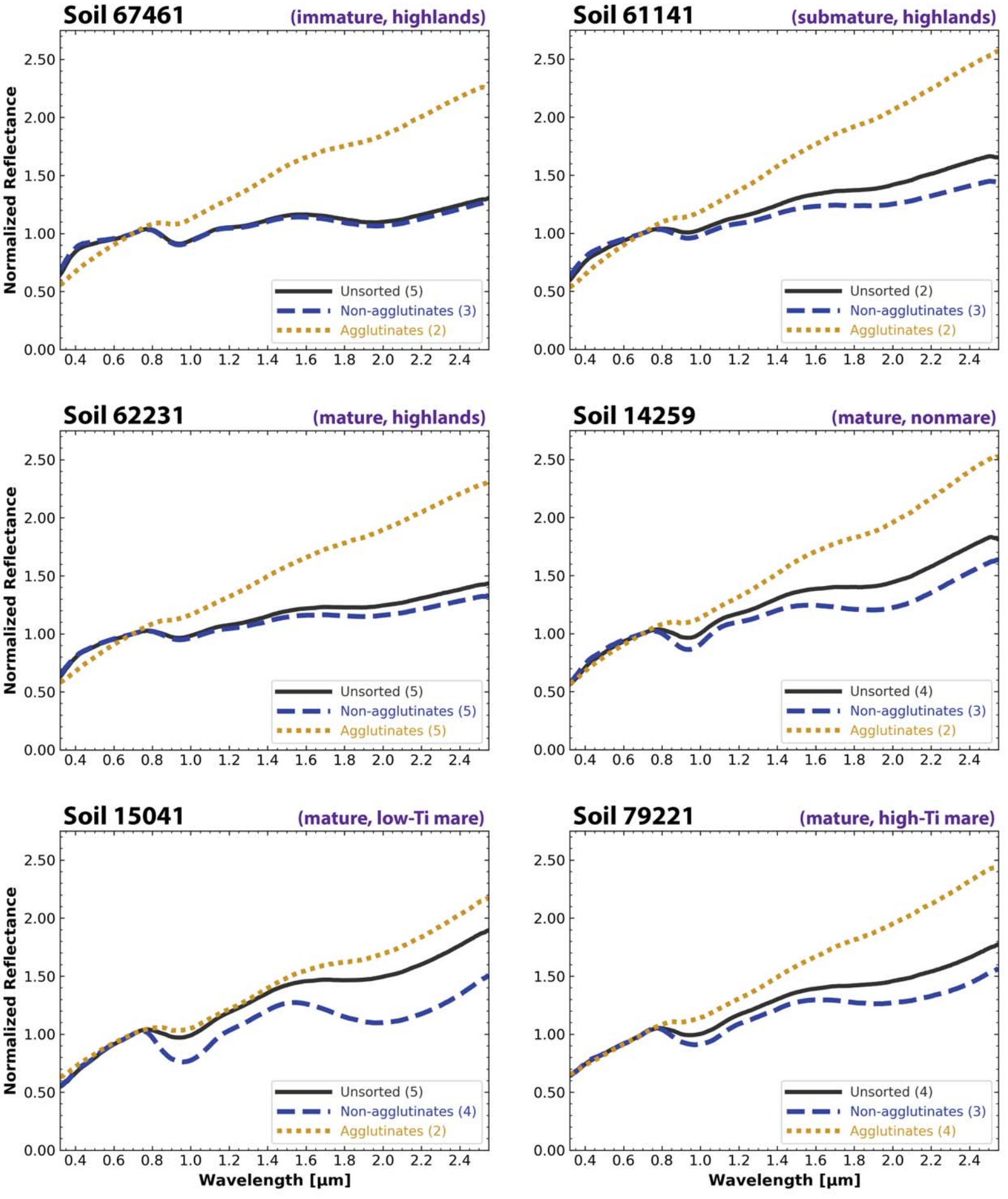
Soil 67461
(immature, highlands)
Unsorted (5)
Non-agglutinates (3)
Agglutinates (2)
Soil 61141
(submature, highlands)
Unsorted (2)
Non-agglutinates (3)
Agglutinates (2)
Soil 62231
(mature, highlands)
Unsorted (5)
Non-agglutinates (5)
Agglutinates (5)
Soil 14259
(mature, nonmare)
Unsorted (4)
Non-agglutinates (3)
Agglutinates (2)
Soil 15041
(mature, low-Ti mare)
Unsorted (5)
Non-agglutinates (4)
Agglutinates (2)
Soil 79221
(mature, high-Ti mare)
Unsorted (4)
Non-agglutinates (3)
Agglutinates (4)
Normalized Reflectance
Wavelength [µm]

Figure 11.

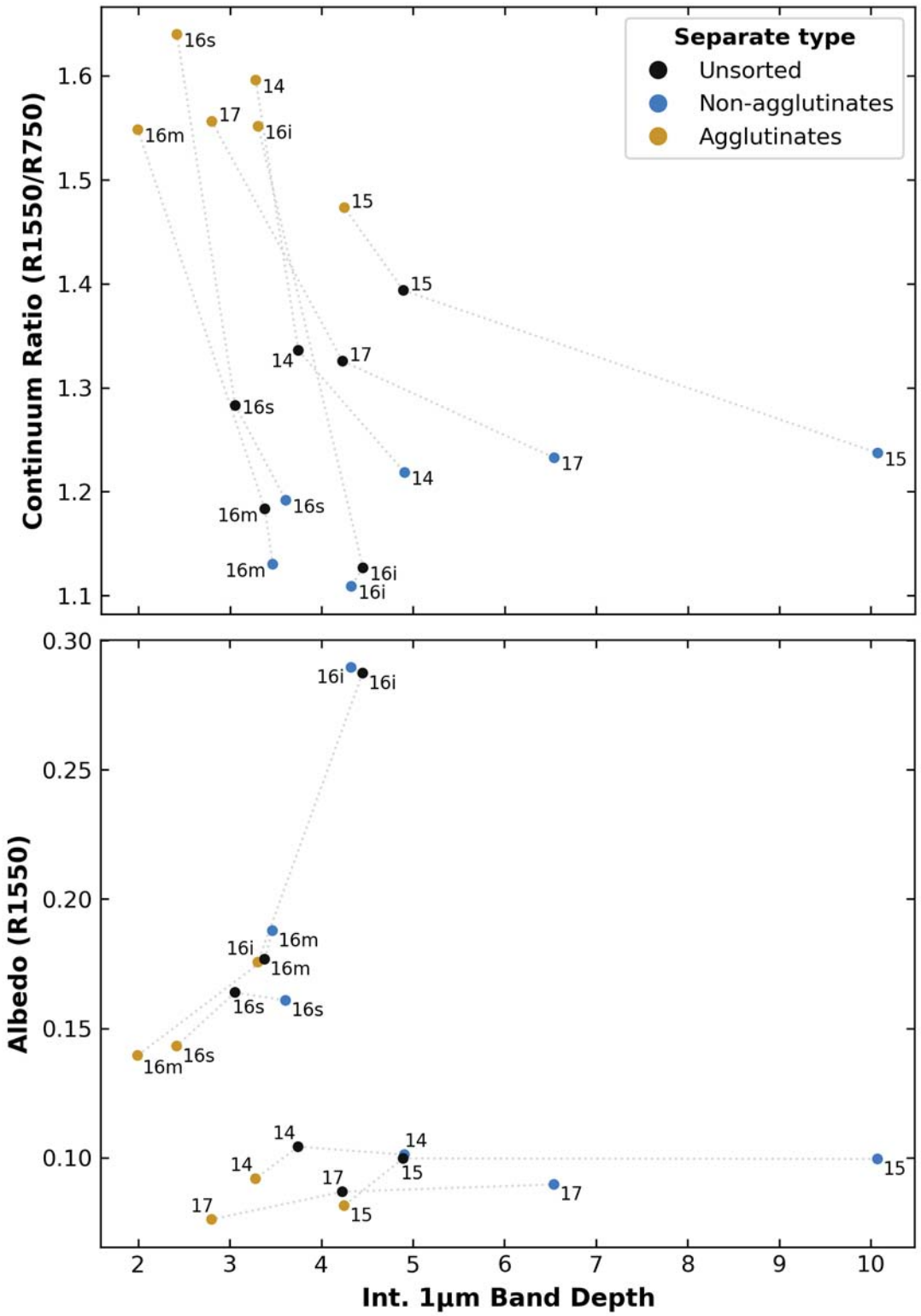
Separate type
Unsorted
Non-agglutinates
Agglutinates
Continuum Ratio (R1550/R750)
Albedo (R1550)
Int. 1µm Band Depth
16s
14
16m
17
16i
15
16s
16m
16i
16i
16m
16m
16s
16s
16m
16s
14
14
17
15
17
15
17
15

Figure 12.

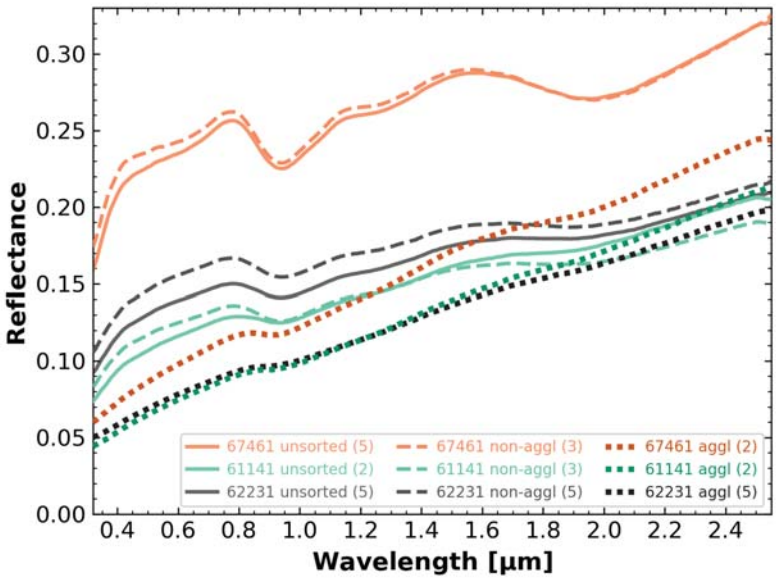
Reflectance
Wavelength [µm]
67461 unsorted (5)
67461 non-aggl (3)
67461 aggl (2)
61141 unsorted (2)
61141 non-aggl (3)
61141 aggl (2)
62231 unsorted (5)
62231 non-aggl (5)
62231 aggl (5)

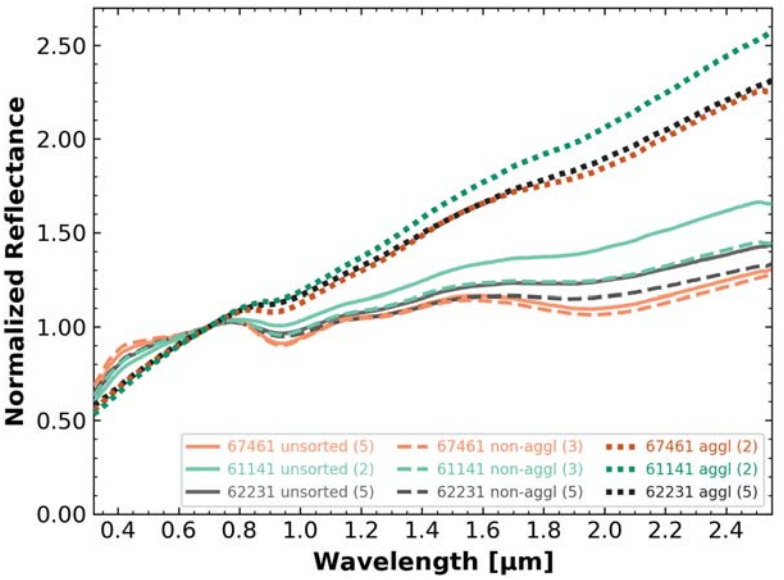
Normalized Reflectance
Wavelength [µm]
67461 unsorted (5)
67461 non-aggl (3)
67461 aggl (2)
61141 unsorted (2)
61141 non-aggl (3)
61141 aggl (2)
62231 unsorted (5)
62231 non-aggl (5)
62231 aggl (5)

Figure 13.

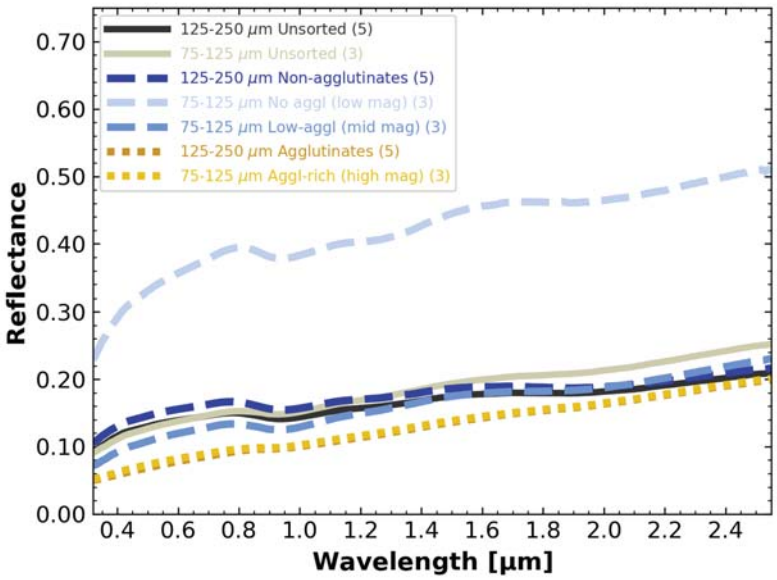
125-250 μm Unsorted (5)
75-125 μm Unsorted (3)
125-250 μm Non-agglutinates (5)
75-125 μm No aggl (low mag) (3)
75-125 μm Low-aggl (mid mag) (3)
125-250 μm Agglutinates (5)
75-125 μm Aggl-rich (high mag) (3)
Reflectance
Wavelength [μm]

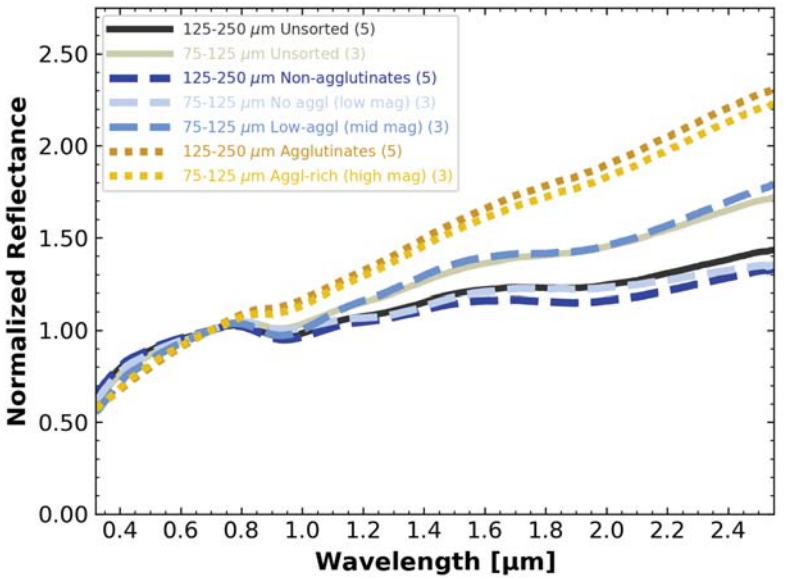
125-250 μm Unsorted (5)
75-125 μm Unsorted (3)
125-250 μm Non-agglutinates (5)
75-125 μm No aggl (low mag) (3)
75-125 μm Low-aggl (mid mag) (3)
125-250 μm Agglutinates (5)
75-125 μm Aggl-rich (high mag) (3)
Normalized Reflectance
Wavelength [μm]

Figure 14.

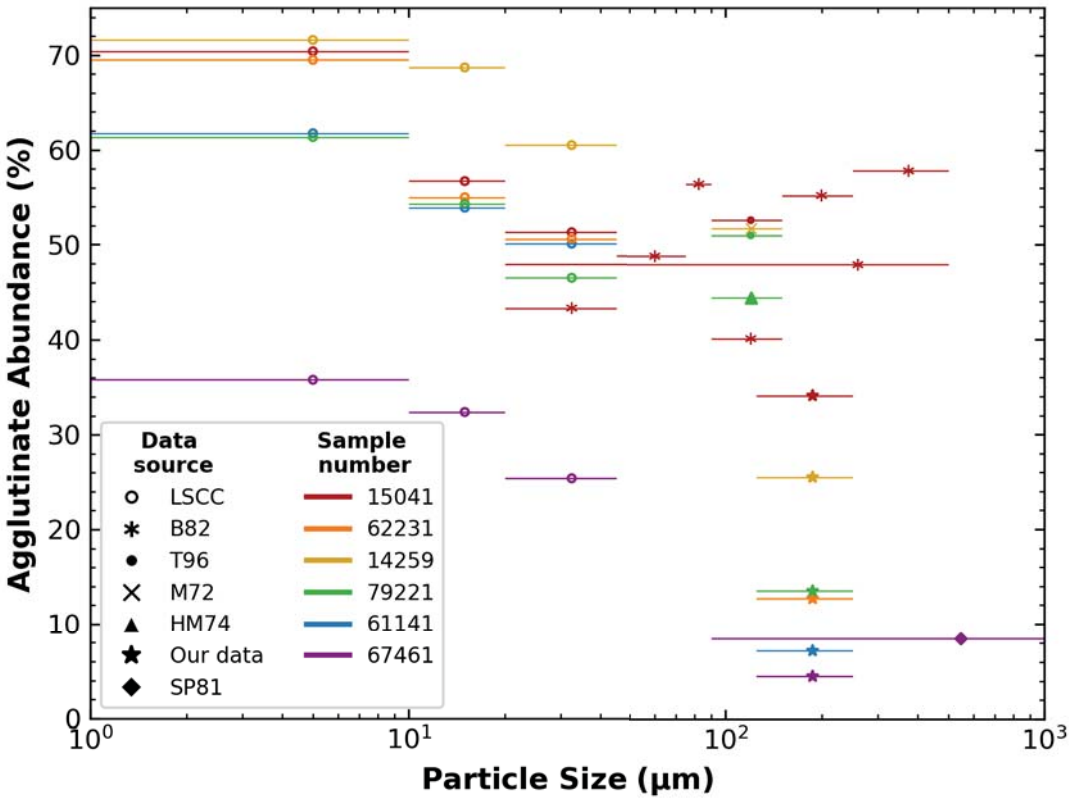
Agglutinate Abundance (%)
Particle Size (μm)
Data source
LSCC
B82
T96
M72
HM74
Our data
SP81
Sample number
15041
62231
14259
79221
61141
67461

Figure 15.

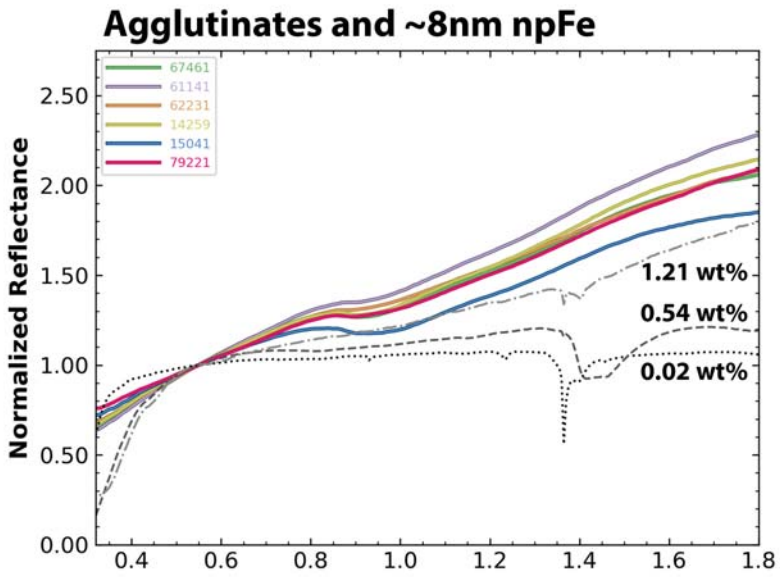
Agglutinates and ~8nm npFe
67461
61141
62231
14259
15041
79221
1.21 wt%
0.54 wt%
0.02 wt%
Normalized Reflectance

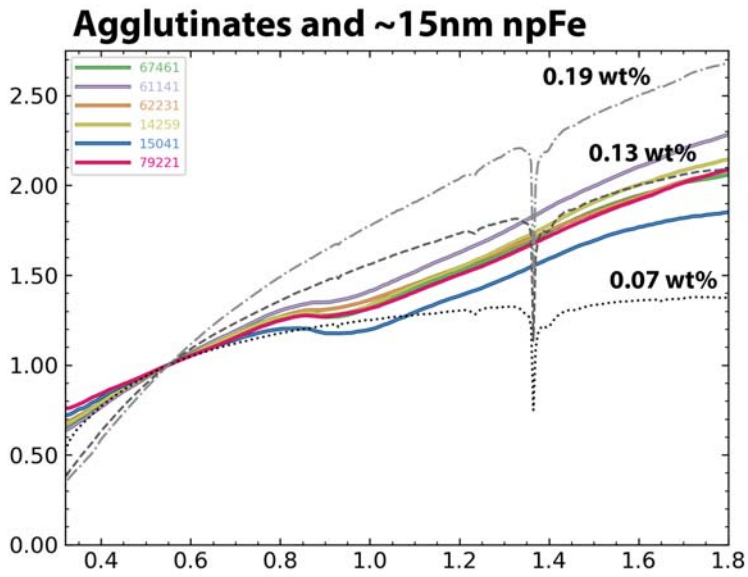
Agglutinates and ~15nm npFe
67461
61141
62231
14259
15041
79221
0.19 wt%
0.13 wt%
0.07 wt%

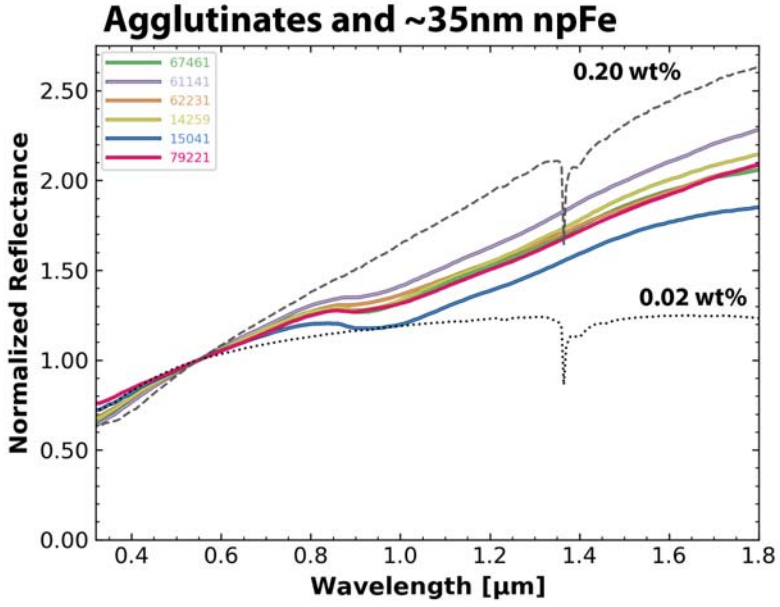
Agglutinates and ~35nm npFe
67461
61141
62231
14259
15041
79221
0.20 wt%
0.02 wt%
Normalized Reflectance
Wavelength [μm]

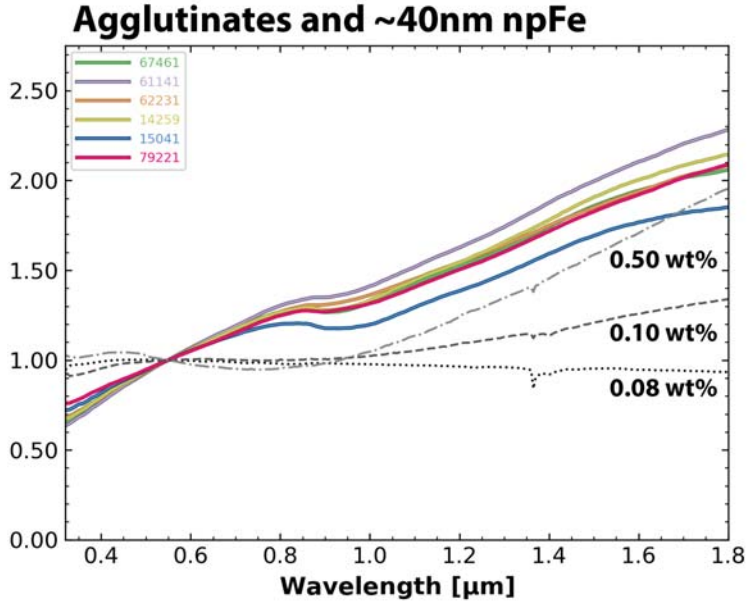
Agglutinates and ~40nm npFe
67461
61141
62231
14259
15041
79221
0.50 wt%
0.10 wt%
0.08 wt%
Wavelength [μm]